balt3/zbc-bc/zbc-bc/zbc00605/zbc8644-05g eichelbt S=4 28/12/04 19:27 4/Color Figure(s) 2-8 ARTNO: M409701200

THE JOURNAL OF BIOLOGICAL CHEMISTRY Vol. 280, No. ??, Issue of ??? ??, pp. 1-xxx, 2005

Printed in U.S.A.

Local Activation of Rap1 Contributes to Directional Vascular Endothelial Cell Migration Accompanied by Extension of Microtubules on Which RAPL, a Rap1-associating Molecule, Localizes*[S]

Received for publication, August 24, 2004, and in revised form, November 23, 2004
Published, JBC Papers in Press, November 29, 2004, DOI 10.1074/jbc.M409701200

Hisakazu Fujita, Shigetomo Fukuhara, Atsuko Sakurai, Akiko Yamagishi, Yuji Kamioka, Yoshikazu Nakaoka, Michitaka Masuda, Naoki Mochizuki‡

From the Department of Structural Analysis, National Cardiovascular Center Research Institute, Suita, Osaka 565-8565, Japan

Endothelial cell migration is promoted by chemoattractants and is accompanied with microtubule extension toward the leading edge. Cytoskeletal microtubules polarize to function as rails for delivering a variety of molecules by motor proteins during cell migration. It remains, however, unclear how directional migration with polarized extension of microtubules is regulated. Here we report that Rap1 controls the migration of vascular endothelial cells. We found that Rap1-associating molecule, RAPL, which belongs to the Ras association domain family (Rassf), localized on microtubules and that activated Rap1 induced dissociation of RAPL from microtubules. A Rap1 activation-monitoring probe based on the fluorescence resonance energy transfer enabled us to demonstrate that local Rap1 activation occurs at the leading edge of the cells under the two types of cell migration, chemotaxis and wound healing. Time lapse imaging of microtubules marked by enhanced green fluorescent protein (EGFP)-RAPL showed the directional growth of microtubules toward the leading edge of the migrating cells. Using adenovirus, inactivation of Rap1 by expression of rap1GAPII inhibited wound healing. In addition, disconnection of Rap1 and RAPL by expression of a RAPL mutant also perturbed wound healing. Collectively, the locally activated Rap1 and its association with RAPL controls the directional migration of vascular endothelial cells.

AQ: A

Rap1 belongs to the Ras GTPase family and cycles between a GDP-bound inactive form and a GTP-bound active form (1). Rap1 activation is regulated by guanine nucleotide exchange factor (GEF),[1] whereas Rap1 inactivation is regulated by GTPase-activating protein (GAP). GEFs contain a catalytic domain and regulatory domains that either bind to upstream molecules or are regulated by second messengers such as cAMP and Ca^{2+}. The former GEFs include C3G and PDZ-GEF; the latter includes CalDAG-GEFs and Epac (cAMP-GEF) (reviewed in Ref. 2). Thus, the spatial Rap1 activation depends on the localization of GEF and the spreading of second messengers. Like GEFs, the spatial Rap1 inactivation depends on the localization of GAPs for Rap1 (3). We have currently developed a spatio-temporal activation/inactivation monitoring probe for Rap1 in living cells (4).

Fn1

Once activated by GEFs, GTP-bound Rap1 associates with effector molecules including Raf-1, B-Raf, RalGDS, and AF-6 (2). Rap1 shares these effector molecules with Ras protein; therefore, Rap1 is suggested to function antagonistically on the Ras-activated intracellular signaling pathway. However, Rap1 may have a unique function in regulating cell adhesion (5, 6). Rap1 was recently reported to be indispensable for cell-extracellular matrix (ECM) contacts by stabilizing the cell-ECM contacts, indicating that Rap1 enhances cell adhesion to ECM (7, 8). Moreover, Bud1, the yeast homologue of Rap1, determines the budding site (9), and Rap1 regulates adherens junction positioning for cell division in *Drosophila* (10), implying that Rap1 is also involved in cell polarization.

Cells have a polarity determined by cell protrusions and retractions, when moving toward certain chemoattractants or during wound healing. In the protrusions, actin is actively polymerized and depolymerized, whereas in retractions stabilized actin fibers are observed (11). For perpetual moving toward the chemoattractants, asymmetrical polarity of cell contacts to ECM is required. Focal adhesions connecting actin stress fibers are assembled in the protrusions and disassembled in the retractions of migrating cells (reviewed in Ref. 12). Like actin, microtubules are assembled toward the leading edge of the protrusions. By constituting rails for motor proteins carrying the molecules to the protrusive part of the cell, microtubule promotes cell polarity (13). Furthermore, recently, assembly and disassembly of focal adhesions are reportedly regulated by microtubules (14, 15). Thus, microtubule extension toward the leading edge parallels the change in polarity of the motile cells toward the chemoattractants or during wound

* This work was supported by grants from the Ministry of Health, Labor, and Welfare of Japan; from the Promotion of Fundamental Studies in Health Science of the Organization for Pharmaceutical Safety and Research of Japan; from the Ministry of Education, Science, Sports and Culture of Japan; from the Cell Science Research Foundation; and from the Mochida Memorial Foundation for Medical and Pharmaceutical Research. The costs of publication of this article were defrayed in part by the payment of page charges. This article must therefore be hereby marked "*advertisement*" in accordance with 18 U.S.C. Section 1734 solely to indicate this fact.

[S] The on-line version of this article (available at http://www.jbc.org) contains two additional figures and eight videos.

‡ To whom correspondence should be addressed: Dept. of Structural Analysis, National Cardiovascular Center Research Institute, 5-7-1 Fujishirodai, Suita, Osaka 565-8565, Japan. Tel.: 81-6-6833-5012 (ext. 2508); Fax: 81-6-6835-5461; E-mail: nmochizu@ri.ncvc.go.jp.

[1] The abbreviations used are: GEF, guanine nucleotide exchange factor; CFP, cyan fluorescent protein; ECM, extracellular matrix; EGFP, enhanced green fluorescent protein; FRET, fluorescence resonance energy transfer; GAP, GTPase-activating protein; GFP, green fluorescent protein; GST, glutathione *S*-transferase; HAEC, human aortic endothelial cell; HUVEC, human umbilical vein endothelial cell; MTOC, microtubule-organizing center; Rassf, Ras association domain family; S1P, sphingosine 1-phosphate; SDF-1, stromal-derived factor-1; YFP, yellow fluorescent protein; MES, 4-morpholineethanesulfonic acid.

healing.

RAPL/NORE1B (hereafter referred to as RAPL) is identified as a Rap1-binding molecule (16), which contains a Ras/Rap1 binding domain and belongs to the Ras association domain family (Rassf) (17, 18). Whereas Rassf members function as potent suppressor of tumors (19–21), RAPL links Rap1 activation upon T cell receptor cross-linking and stromal-derived factor-1 (SDF-1) stimulation to integrin activation. In addition, RAPL mediates the polarized distribution of SDF-1 receptors upon Rap1 activation (16). Recently, Rassf1 has been shown to localize at and stabilize microtubules (22). However, it is unclear whether other molecules belonging to Rassf function in the association with Ras family GTPases.

We investigate the localization of RAPL in the vascular endothelial cells and how Rap1-RAPL participates in determining the directional migration in response to a chemoattractant, sphingosine 1-phosphate (S1P) (23), and during wound healing. RAPL localizes at the microtubule-organizing center (MTOC) and microtubules. Rap1 is activated at the leading edge of migrating cells. In addition, inactivation of Rap1-RAPL signal perturbed the wound closure. These data suggest that local activation of Rap1 and its association with RAPL regulates the directional cell migration of vascular endothelial cells.

EXPERIMENTAL PROCEDURES

Reagents and Antibodies—S1P was purchased from Biomol (Plymouth, PA). Protein A-Sepharose was from Calbiochem. Anti-green fluorescent protein (GFP) was developed in our laboratory. Anti-β-tubulin, anti-γ-tubulin, and anti-FLAG (M2) were purchased from Sigma, and anti-Rap1 was from BD Biosciences. Anti-RAPL antibody was a kind gift from T. Kinashi (Kyoto University, Japan).

Plasmids—The coding sequences of human Rassf1A, Rassf1C, Rassf2 (KIAA0168), Rassf3, and RAPL (NORE1B) were amplified by PCR using human heart cDNA library as a template. pCA-EGFP-Rassf1A, -Rassf1C, -Rassf2, -Rassf3, and RAPL were derived from pCAGGS eukaryotic expression vector and expressed enhanced green fluorescent protein (EGFP)-tagged each Rassf molecules (24). cDNAs encoding RAPL deletion mutants as indicated in Fig. 4 were amplified by PCR and ligated into pCA-EGFP vector similarly to Rassf1. dC1, dC2, dC3, and dN encoded amino acids 1–222, 1–168, 1–100, and 101–265 of RPAL, respectively. A mutant of RAPL (hereafter referred to as the RA mutant), in which Lys^{123}, Arg^{124}, Lys^{135}, Lys^{154}, Lys^{155}, Asp^{160}, and Asn^{161} were replaced with Ala, was reported to be incapable of associating with Rap1 (16). cDNA encoding an RA mutant was amplified by PCR-based mutagenesis and subcloned into pCA-EGFP. pCXN2-FLAG-Rap1 expressed FLAG-tagged Rap1. Either constitutive active or dominant negative forms of Rap1 (Rap1V12 or Rap1N17) cDNAs were similarly inserted into pCXN2-FLAG. pIRM21-Rap1V12 expressed FLAG-tagged Rap1V12 and internal ribosomal entry site-driven dsFP593 as described previously (24). pIRM21-rap1GAPII expressed both FLAG-tagged rap1GAPII and internal ribosomal entry site-driven dsFP593. pCA-DsRed-CrkI was derived from pCAGGS eukaryotic expression vector as described previously (24). pRaichu-Rap1, a Rap1 activation monitoring probe based on fluorescence resonance energy transfer (FRET), was described previously (4). pRaichu-Rap1 expressed a chimeric protein consisting of yellow fluorescent protein (YFP), Rap1, and Ras-binding domain of Raf and cyan fluorescent protein (CFP) followed by the CAAX motif of Ki-Ras. In pRaichu-Rap1N17, a cDNA encoding Rap1N17 was replaced with that encoding Rap1. pGEX-RAPL was constructed by inserting a cDNA encoding full-length RAPL into pGEX (Amersham Biosciences).

Adenovirus—Both an adenovirus-expressing EGFP-tagged RAPL and an adenovirus-expressing EGFP-tagged RA mutant of RAPL were produced using the Adeno-X expression system (BD Biosciences). Briefly, cDNA from pCA-EGFP-RAPL was inserted into Adeno-X viral DNA using pShuttle as a transfer vector. Adenovirus-expressing EGFP-RAPL was produced from HEK293 cells transfected with Adeno-X-EGFP-RAPL. An adenovirus-expressing RA mutant of RAPL was produced in a similar manner to RAPL-expressing adenovirus. The EGFP-expressing adenovirus and the rap1GAPII-expressing adenovirus were generous gifts from H. Kurose (Kyushu University, Japan) and S. Hattori (Tokyo University, Japan), respectively.

Cell Culture and Transfection—Human umbilical vein endothelial cells (HUVECs) and human aortic endothelial cells (HAECs) were purchased from Cascade Biologics, Inc. (Portland, OR) and cultured in Humedia-EG2 as previously reported (24). HEK293T cells were generous gifts from Dr. B. J. Mayer (University of Connecticut) and maintained as described previously. Jurkat cells and HEK293 cells were obtained from the American Type Culture Collection (Manassas, VA) and cultured in RPMI 1640 (Invitrogen) and Dulbecco's modified Eagle's medium supplemented with 10% fetal bovine serum. Cultured cells were transfected using Lipofectamine 2000 reagent (Invitrogen).

Reverse Transcription-PCR, Pull-down Assay, Immunoprecipitation, and Immunoblotting—RNAs from cultured Jurkat cells and HUVECs were prepared by TRIzol (Invitrogen). cDNAs was synthesized by reverse transcriptase reaction using random primer and RNAs as templates. The cDNA specific for human RAPL was amplified by PCR using a primer set (5′RAPL, CTGGACGAGGAACTGGAAGACTGCTTC; 3′RAPL, AGGGATGGAGAAGGCATCCCACTCTAC). GTP-bound Rap1 was detected according to the method of Bos and co-workers (25). Briefly, HUVECs stimulated with 1 μM S1P for the time indicated at the *top* of the figure were lysed in lysis buffer (50 mM Tris, pH 7.5, 150 mM NaCl, 5 mM $MgCl_2$, 1% Nonidet P-40, 0.1% SDS, 0.5% deoxycholic acid, 1 mM Na_3VO_4). Precleared lysates were incubated with GST-Rap1-binding domain of RalGDS and glutathione-Sepharose beads. Proteins collected on the beads were subjected to SDS-PAGE followed by immunoblotting with anti-Rap1 antibody. Immunoprecipitation and immunoblotting were performed as described previously (26). Briefly, HEK293T transfected with plasmids as indicated in the figures were lysed using lysis buffer. Lysates were precleared by centrifugation at 15,000 × *g* for 10 min, followed by immunoprecipitation using anti-GFP and Protein A-Sepharose. Immunoprecipitates were subjected to SDS-PAGE and immunoblotting with anti-FLAG antibody and peroxidase-conjugated goat anti-mouse IgG as a primary and a secondary antibody, respectively. Proteins reacting with anti-FLAG were visualized by an ECL system (Amersham Biosciences) and an LAS-1000 system (Fuji Film, Japan).

Microtubule Binding Assay—Microtubule-associating protein-containing microtubule fractions prepared from bovine brain were gifts from N. Yamagishi (Kyoto Pharmaceutical University, Japan). Glutathione *S*-transferase-fused RAPL (GST-RAPL) expressed in BL21-Star bacteria (Invitrogen) was collected on glutathione-Sepharose (Amersham Biosciences). GST-RAPL was eluted using 10 mM glutathione, precleared by centrifugation at 400,000 × *g*, and polymerized in microtubule-binding buffer (100 mM MES-KOH (pH 6.8), 2 mM EDTA, 1 mM $MgCl_2$, 10 mM Taxol, 4 M glycerol, and 1 mM GTP). For the microtubule binding assay, 5 μg of purified microtubules and GST-RAPL at the concentration indicated in the figure legends were mixed in 200 μl of microtubule-binding buffer for 30 min at 37 °C. After centrifugation at 400,000 × *g* for 15 min, equal amounts of the supernatant and the pellet were analyzed by SDS-PAGE and immunoblotting with anti-GST. Bovine serum albumin fraction V was used as a negative control for GST-RAPL.

Wound Healing Assay and Responses to Chemoattractant from a Micropipette—HUVECs or HAECs transfected with plasmids indicated in the figures were cultured on 35-mm glass bottom dishes coated with collagen until they reached the monolayer state. The cells were scratched by a regular 20-μl pipette tip along the diameter of the bottom glass. The culture medium remained unchanged during wound healing. Monolayer-cultured HUVECs infected with an adenovirus expressing rap1GAPII, an adenovirus expressing EGFP-RAPL, or an adenovirus expressing the RA mutant of RAPL were scratched and time lapse-imaged. HAECs expressing EGFP-RAPL or those expressing Raichu-Rap1 cultured on glass-bottom dishes coated with collagen were exposed to 1 μM S1P supplied by a micropipette (FemtoJet; Eppendorf Japan).

Fluorescence Microscopy and Confocal Imaging—HUVECs or HAECs transfected with plasmids expressing fluorescence-tagged proteins as indicated in the figure legends were imaged on an Olympus IX-81 inverted microscope. The microscope with a 75-watt xenon arc lamp was equipped with a cooled charge-coupled device camera, CoolSNAP-HQ (Roper Scientific), and two filter exchangers, controlled by MetaMorph 5.0 software (Molecular Devices). The EGFP image and DsRed image were obtained through an XF2043 dichroic filter (Omega) and either a set of an S484/15 excitation filter and an S515/30 emission filter or a set of an S555/25 excitation filter and an S630/60 emission filter, respectively, as reported previously (27). HUVECs transfected with pCA-EGFP-RAPL cultured on a collagen-coated glass-base dish were fixed by 4% paraformaldehyde at room temperature, followed by permeabilization with 0.1% Triton X-100. Permeabilized cells were incubated with anti-β-tubulin or anti-γ-tubulin antibody. Immunopositive reaction was visualized with Alexa 546 goat-anti-mouse IgG (Mo-

balt3/zbc-bc/zbc00605/zbc8644-05g eichelbt S=4 28/12/04 19:27 4/Color Figure(s) 2-8 ARTNO: M409701200

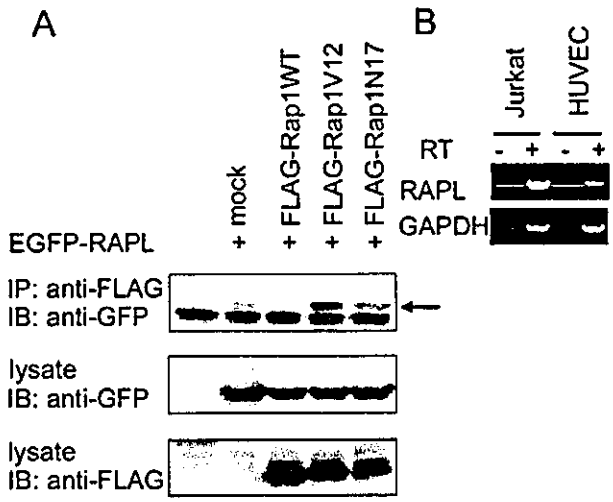

FIG. 1. **The association of RAPL with Rap1 and its expression in vascular endothelial cells.** *A*, HEK293T cells were transfected with plasmids as indicated at the *top*. Cell lysates were subjected to immunoprecipitation (*IP*) followed by immunoblotting (*IB*) with antibodies as indicated on the *left* or directly subjected to SDS-PAGE followed by immunoblotting with the antibodies as indicated on the *left*. An *arrow* denotes GTP-bound Rap1 co-immunoprecipitated with EGFP-tagged RAPL. *B*, RNA prepared from the cells as indicated at the *top* was subjected to reverse transcription-PCR analysis. The sequence of RAPL-specific primers is described under "Experimental Procedures." RNA from Jurkat cells was used as a positive control. The results are representative of more than three independent experiments.

lecular Probes, Inc., Eugene, OR). Confocal images of EGFP and Alexa 546 were obtained by an Olympus BX50WI microscope controlled by Fluoview. To monitor the cell shape and localization of fluorescence-tagged molecules in living cells, a phase-contrast image and a fluorescence image were obtained every 20 s. A series of time lapse images were converted into video format using MetaMorph 5.0.

Imaging of Rap1 Activation in Living Cells—HAECs cultured on collagen-coated 35-mm diameter glass base dishes were transfected with pRaichu-Rap1 and observed after scratching. Cells similarly transfected with pRaichu-Rap1 were observed during exposure to 1 μM S1P supplied by a micropipette. The structure of Raichu-Rap1 and the principle of FRET is illustrated as in Fig. 5*D*. Cells were imaged on an Olympus IX-81 inverted fluorescence microscope in a method similar to fluorescence imaging as described previously (24). Dual images for CFP and YFP were obtained through an XF1071 excitation filter, an XF2034 dichroic filter, and an XF3075 emission filter for CFP and an XF3079 for YFP (Omega), respectively. The ratio image of YFP/CFP were created by MetaMorph 5.0 software and displayed as an intensity-modulated display image as described previously (4).

RESULTS

A Rap1-binding Protein, RAPL, Is Expressed in Vascular Endothelial Cells—RAPL associates with Rap1 upon T-cell receptor stimulation or chemokine stimulation, resulting in redistribution of integrin in lymphocytes (16). Vascular endothelial cells and hematopoietic cells originate from common hemangioblasts; therefore, we tested whether vascular endothelial cells express RAPL, since Jurkat cells express RAPL (16). RAPL expression was examined by reverse transcription-PCR analysis using a RAPL-specific primer set. HUVECs expressed RAPL mRNA similarly to Jurkat cells used as a positive control (Fig. 1*A*). We further examined the association of GTP-Rap1 with RAPL by the co-immunoprecipitation assay using 293T cells (Fig. 1*B*). F1

A member of Rassf1A localizes to microtubules in COS cells (22), whereas the localization of RAPL has not yet been clearly demonstrated, although it is reported to accumulate at the leading edge of T lymphocytes (16). Thus, we tested the localization of RAPL in the vascular endothelial cells by using EGFP-tagged RAPL. Rassf members as listed (Fig. 2*A*) were tagged with EGFP and expressed in HAECs. All Rassf members contain the Ras- and Rap1-binding domain (RA domain) (Fig. 2*A*). The expression of EGFP-tagged Rassfs was confirmed by the immunoblot analysis from the lysates of HEK293T cells transfected with the plasmids as indicated at the *top* (Fig. 2*B*). EGFP-tagged Rassf1A and -1C, splicing variants from the same gene, were found as circular fibers in the central region of cells except the nucleus, whereas EGFP-tagged Rassf3 and EGFP-RAPL were found as fibers emanating from the central to the periphery. These results suggested that the circular fibers on which EGFP-tagged Rassf1A and -1C localized may represent microtubules deformed by Rassf1-induced stabilization, as previously demonstrated (22). Rassf3 and RAPL appeared to localize on normal microtubules originating from MTOC to the periphery. Thus, we examined the colocalization of EGFP-RAPL with β-tubulin-constituting microtubules and with γ-tubulin preferably localized on MTOC. As expected, EGFP-RAPL clearly localized on microtubules from the MTOC to the periphery (Fig. 2*D*). In clear contrast to these fibrous expressions, EGFP-Rassf2 was found exclusively in the nucleus. We compared the EGFP-RAPL with EGFP-Rassf1A expressed in motile vascular endothelial cells using time lapse imaging. Both RAPL-expressing cells and Rassf1A-expressing cells showed membrane ruffling (Supplemental Video 1); however, microtubules marked by EGFP-RAPL moved dynamically as regular microtubules, whereas those marked by EGFP-Rassf1 were static (Supplemental Video 2). These data indicated that Rassf members, Rassf3 and RAPL, appear to bind to microtubules without affecting the endogenous microtubule structure. F2

We further confirmed the localization of RAPL on microtubules by immunostaining using anti-RAPL antibody. Endogenous RAPL localized on microtubules in HAECs (Fig. 3*A*). The association of RAPL and microtubules were examined by biochemical analysis using purified microtubules and GST-RAPL. The microtubule binding assay revealed that GST-RAPL cosedimented with microtubules in a concentration-dependent manner. Although GST-RAPL and tubulin closely migrated in SDS-PAGE (Fig. 3*B*, *top panel*), GST-RAPL was clearly separated by immunoblotting with anti-GST (Fig. 3*B*, *middle panel*). In agreement with these observations, when microtubule formation was inhibited by nocodazole, the filamentous expression of RAPL was not observed (Supplemental Fig. 1). Collectively, these results indicated that endogenous RAPL localizes on microtubules in vascular endothelial cells. F3

RAPL Requires Rap1-associating Domain for Localizing on Microtubules, but Not Its Association with Rap1—To define the region responsible for the association of RAPL with microtubules, we constructed a series of truncated mutants and a mutant incapable of associating with Rap1 (RA mutant) (Fig. 4*A*). The expression of EGFP-tagged RAPL and its mutants was confirmed by the immunoblot analysis from the lysates of HEK293T cells transfected with the plasmids as indicated at the *top* of Fig. 4*B*. We examined the expression of EGFP-tagged RAPL and its mutants in HAECs (Fig. 4*C*). EGFP-tagged full-length RAPL and coiled-coil domain-lacking mutant (dC1) localized on microtubules. Intriguingly, RA mutant also localized on microtubules. However, neither RA domain-lacking mutant (dC2 and dC3) nor a mutant lacking the amino-terminal 100 amino acids (dN) localized on microtubules. The EGFP-tagged RA domain alone was not expressed on the microtubules. These data indicated that the association of RAPL with Rap1 is not required for the localization of RAPL on microtubules and that the amino-terminal part of RAPL and the RA domain are essential for its targeting to microtubules. F4

balt3/zbc-bc/zbc-bc/zbc00605/zbc8644-05g eichelbt S=4 28/12/04 19:27 4/Color Figure(s) 2–8 ARTNO: M409701200

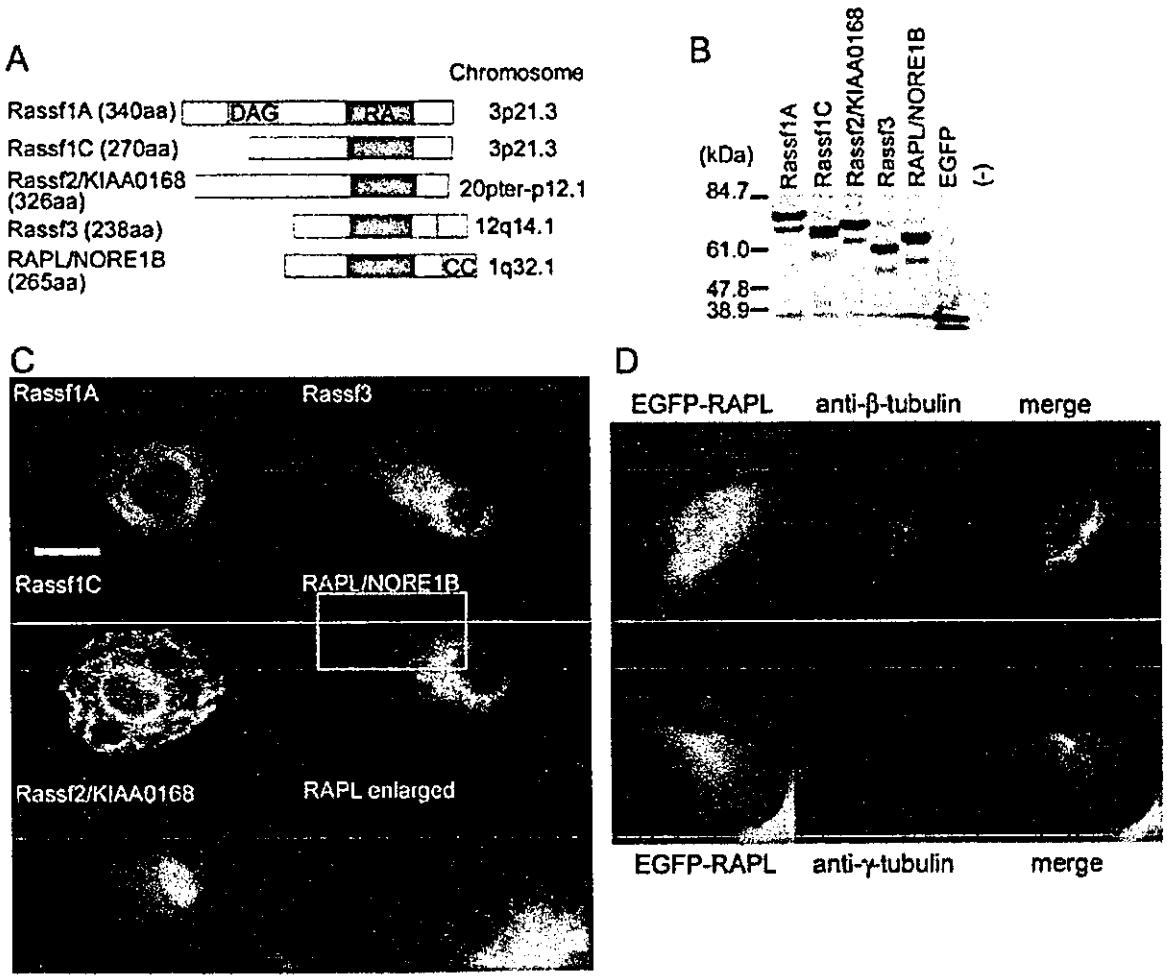

AQ: M FIG. 2. **RAPL localizes to the microtubules in vascular endothelial cells.** *A*, Rassf members are schematically illustrated. All Rassfs contain a Ras/Rap1-associating domain (*RA*). Only Rassf1A contains the diacylglycerol-binding motif (*DAG*). Rassf3 and RAPL have coiled-coil domain (*CC*) in the carboxyl terminus. The localization of each gene to human chromosome is indicated on the *right*. *aa*, amino acids. *B*, HEK293T cells were transfected with EGFP-tagged plasmids as indicated at the *top*. Cell lysates were subjected to SDS-PAGE followed by immunoblotting with anti-GFP. –, untransfected. Molecular weight markers are indicated on the *left*. *C*, HAECs were transfected with the plasmids used in *B* and imaged through an Olympus IX81 fluorescent microscope. Note that EGFP-tagged Rassf1A and Rassf1C localize on the spiral fibers, whereas EGFP-tagged Rassf3 and RAPL localize at fibrous structures emanating from the center of the cell to the periphery. The tubular structure observed in HAECs expressing EGFP-RAPL is enlarged in the *right bottom panel*. Motile HAECs transfected with either EGFP-Rassf1A or EGFP-Rassf3 were video-imaged for phase contrast and EGFP. A series of phase-contrast images and EGFP images of each cell were converted to two videos, Supplemental Video 1 (phase contrast) and Supplemental Video 2 (EGFP). Elapsed time in video is indicated as h: min. Noticeably, the spiral structure surrounding the nucleus in the cell expressing Rassf1A does not move in the protrusive area at all. In clear contrast, the array from the center to the periphery of the cell expressing EGFP-Rassf3 moves toward the ruffled membrane, although both cells move spontaneously, similar to the untransfected cells. *Bar*, 20 μm. *D*, HAECs expressing EGFP-RAPL plated on a collagen-coated glass base dish were fixed with 4% paraformaldehyde, permeabilized with 0.1% Triton X-100, and incubated with anti-β-tubulin (*top*) or anti-γ-tubulin (*bottom*). Immunoreactive proteins were visualized by Alexa546 goat anti-mouse IgG. Both EGFP and Alexa546 images obtained through a BX50WI confocal microscope controlled by Fluoview are shown as RAPL (*green*), tubulin (*red*), and superimposed (*merge*). Note that EGFP-RAPL localizes on microtubules from the MTOC to the peripheral microtubules. *Bar*, 20 μm.

AQ: I *Rap1 Locally Activated by S1P Triggers Directional Migration Preceding Microtubule Extension*—To understand the significance of Rap1 activation and RAPL localizing on microtubules, we examined RAPL localization in HAECs expressing either Rap1V12 or rap1GAPII. EGFP-RAPL dislocated from microtubules in HAECs expressing Rap1V12, whereas it localizes on microtubules in HAECs expressing rap1GAPII (Fig. 5*A*). These F5 results suggested that activated Rap1 appears to determine the localization of RAPL. Thus, we investigated the effect of local activation of Rap1 on localization of EGFP-RAPL. Since vascular endothelial cells become motile upon S1P stimulation, S1P is thought to function as a chemoattractant (23). S1P did activate Rap1 as demonstrated by pull-down assay (Fig. 5*B*). GTP-Rap1 was increased at 1 min after S1P stimulation, and its activation persisted until 15 min after stimulation.

To examine the orientation of microtubule growth upon local S1P stimulation, we applied S1P to HAECs using micropipette. HAECs expressing EGFP-RAPL were monitored for cell movement and microtubule growth by phase-contrast and EGFP observations, respectively. HAECs cultured on the collagen-coated dish spontaneously moved around and exhibited prominent membrane ruffling, where the microtubules marked by EGFP-RAPL grew forward as shown by the *center panels* of Fig. 5*C*. The same cell was stimulated by 1 μM S1P released from the micropipette tip (Fig. 5*C*, *right panel*). The cell changed the direction of movement and showed remarkable membrane ruffles toward the pipette tip in response to S1P. Notably, microtubules marked by EGFP-RAPL started to grow

balt3/zbc-bc/zbc-bc/zbc00605/zbc8644-05g eichelbt S=4 28/12/04 19:27 | 4/Color Figure(s) 2-8 | ARTNO: M409701200

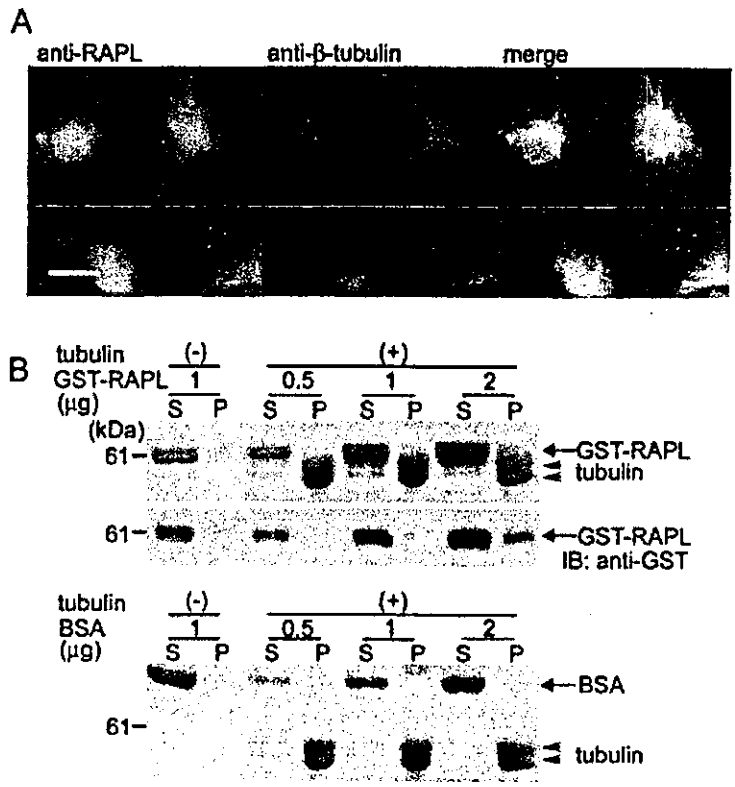

FIG. 3. **RAPL localizes on and binds to microtubules.** *A*, HAECs were immunostained with anti-RAPL antibody (*green*). Microtubules were visualized with immunostaining with anti-β-tubulin (*red*). A *merged image* is shown in the *right panel* (*merge*). *Bar*, 20 μm. *B*, GST-RAPL at the concentration as indicated at the *top* was mixed with 5 μg of purified tubulin (+) or without tubulin (−). After centrifugation at 400,000 × *g* for 30 min at 37 °C, supernatant (*S*) and pellet (*P*) were subjected to SDS-PAGE (*top panel*) followed by immunoblotting (*IB*) with anti-GST (*middle panel*). *Arrows*, *arrowheads*, and a *broken arrow* indicate GST-RAPL, tubulin, and bovine serum albumin (*BSA*), respectively. Note that GST-RAPL cosedimented with microtubules is detected in the pellet. To examine the specificity of the cosedimentation of GST-RAPL with microtubules, bovine serum albumin was used as a negative control in similar analyses to GST-RAPL (*bottom panel*).

in the protrusive area in the U-turned cell. The responses to S1P were constantly observed when HAECs were exposed to S1P from the tip of the micropipette. A series of phase-contrast images and EGFP images were converted to a video (Supplemental Video 3). We further confirmed the requirement of microtubule growth for directional migration by examining whether endothelial cells extend membranes in response to S1P in the presence or absence of nocodazole. Before the nocodazole treatment, endothelial cells responded to S1P and extended their membranes, whereas after nocodazole, the cells did not extend their membranes (Supplemental Video 4). These data indicated that microtubules grow toward the chemoattractant, which promotes the directional cell movement.

To monitor the spatio-temporal activation of Rap1 in response to S1P from a micropipette, HAECs expressing Raichu-Rap1 were subjected to time lapse FRET imaging. Raichu-Rap1 consists of YFP, Rap1, the Ras-binding domain of Raf, CFP, and a CAAX box of Ki-Ras. This probe enabled us to show Rap1 activation by the increased ratio of YFP/CFP, based upon FRET from CFP to YFP (Fig. 5*D*). Raichu-Rap1-expressing HAECs exhibited remarkable membrane ruffles when stimulated with S1P from a micropipette (Fig. 5*E*, *third column*, *top*). At this time point, the increased FRET reflecting Rap1 activation was observed at the ruffled membrane (Fig. 5*E*, *third column*, *bottom*). When S1P was released from the relocated micropipette tip, the same cell responded to S1P and showed membrane ruffles toward the micropipette, similar to the first test. The similar Rap1 activation demonstrated by increased FRET was observed at the ruffled membrane (Fig. 5*E*, *right column*). A video image for both phase-contrast view and that for FRET images is shown as Supplemental Video 5. Rap1 activation at the ruffled membrane upon S1P stimulation was confirmed by the observation that Rap1 was not activated at the ruffled membrane before the S1P stimulation (Supplemental Fig. 2*A*). In addition, FRET observed at the ruffled membrane using Raichu-Rap1 was not detected when Raichu-Rap1N17 was used, although S1P-induced membrane ruffling was observed (Supplemental Fig. 2*B* and Video 6). By stimulating cells with S1P-free media, we also excluded the possibility that fluid pressure or the proximity of the pipette tip to the cell might cause FRET (Supplemental Video 7). These data indicated that chemoattractant-induced local activation of Rap1 may become a trigger of directional migration accompanied with extension of EGFP-RAPL-marked microtubules. AQ: J

Rap1 Activated during Wound Healing Is Accompanied by Microtubule Extension—To assess the consequence of the Rap1 activation and the association of activated Rap1 with RAPL, we examined the activation of RAPL and EGFP-RAPL-marked microtubules during wound healing. Microtubules grow in the protruding region of motile polarizing fibroblasts (28). It has been unclear what determines the polarized growth of microtubules. During wound healing, monolayer vascular endothelial cells migrated to the wound unidirectionally (Fig. 6*A*, *top panels*, phase-contrast observations). Crk is an adaptor protein linking signaling from integrins as well as receptor tyrosine kinases to its Src homology 3 domain-binding proteins via Src homology 2 domain. It localizes at focal adhesions by constituting complexes with Src homology 2 domain-binding partners, paxillin and p130Cas (29, 30). To monitor the focal adhesion assembly and growth of microtubules simultaneously, endothelial cells were transfected with the plasmids expressing DsRed-CrkI and EGFP-RAPL. Before scratching, DsRed-CrkI was punctually expressed in the focal adhesions at the cell periphery and the cell body (Fig. 6*A*, *bottom*, *left panel*). When cells started to move toward the wound, the focal complexes and focal adhesions marked by DsRed-CrkI developed profoundly in the leading edge of the cells (24, 31); meanwhile, those in the retracting region were disassembled (Fig. 6*A*, *bottom*, *right panel*). During cell migration upon scratching, microtubules marked by EGFP-RAPL grew in the protrusive region and FIG

balt3/zbc-bc/zbc-bc/zbc00605/zbc8644-05g eichelbt S=4 28/12/04 19:27 4/Color Figure(s) 2-8 ARTNO: M409701200

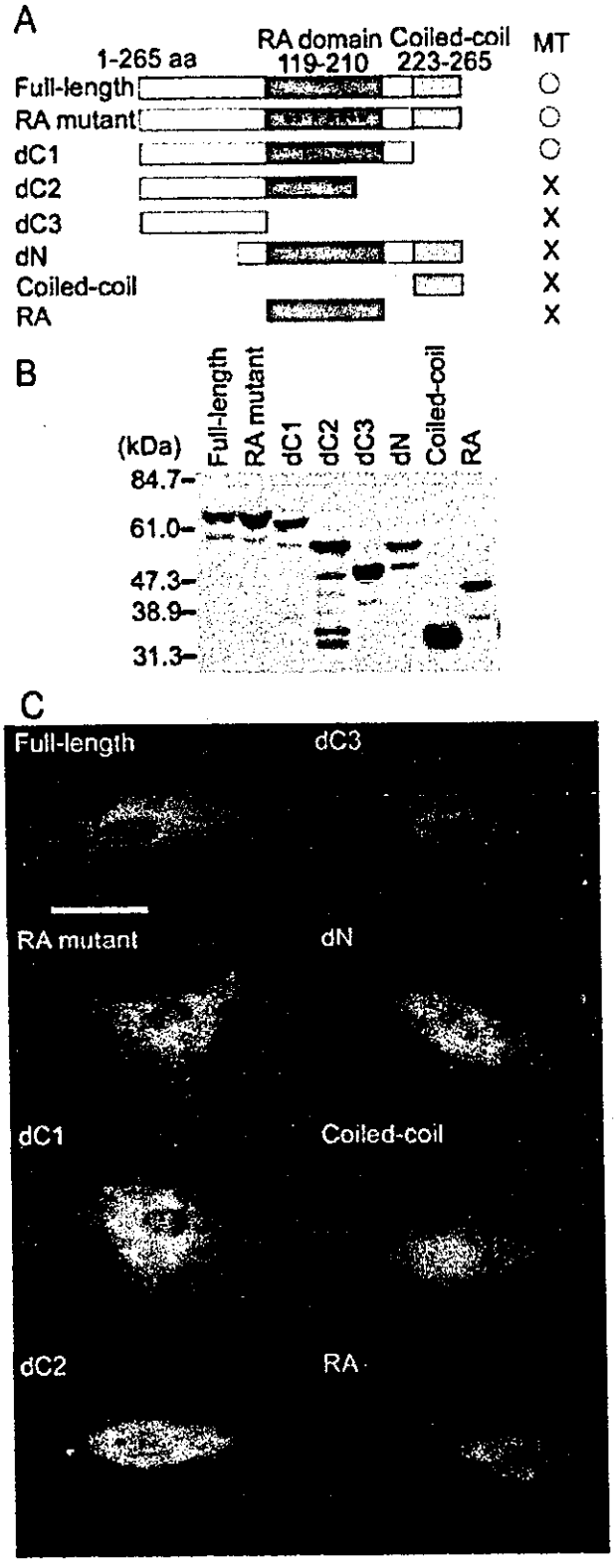

F7

F8

FIG. 4. **The sequence besides the essential amino acids in RA domain required for the association of RAPL with Rap1 is necessary for the localization of RAPL to microtubules.** *A*, schematic illustration of RAPL and its mutants. RAPL consists of an uncharacterized amino terminus, followed by a Ras/Rap1-associating domain (RA domain) and coiled-coil domain. The amino acid (*aa*) number encoding each domain is indicated at the *top*. *RA mutant*, the mutant incapable of associating with Ras and Rap1. The *stars* indicate the seven amino acids required for the association of RAPL with Rap1 that are replaced with Ala. dC1 and dC2 lacks the coiled-coil domain and both the RA domain and the coiled-coil domain, respectively. dC3 consists of the amino-terminal 100 amino acids. dN lacks the amino-terminal 100 amino acids, which have not been characterized. The coiled-coil and the RA consist of the only coiled-coil domain and the RA domain, respectively. The localization of RAPL and its mutants on microtubules is summarized on the *right*. *B*, HEK293T cells were transfected with the plasmids encoding amino-terminally EGFP-tagged DNA, as indicated at the *top*. Cell lysates were subjected to SDS-PAGE, followed by immunoblot probed with anti-GFP antibody. Molecular weight markers are indicated at the *left*. *C*, HAECs transfected with the plasmids used in *B* were imaged using an Olympus IX-81 fluorescent microscope. Note that RA mutant and dC1 localize on microtubules as well as full-length RAPL. *Bar*, 40 μm.

developed toward the leading edge marked by DsRed-CrkI (Fig. 6*A*). A series of images for microtubules marked by EGFP-RAPL and those for focal adhesions marked by DsRed-CrkI were converted to a video file (Supplemental Video 8). We further confirmed that endogenous RAPL localized on microtubules in the protruding area of migrating cells during wound healing (Fig. 6*B*).

Rap1 is activated downstream of Crk via its Src homology 3 domain-binding protein, C3G, which is a GEF for Rap1 (32). Thus, we examined whether Rap1 was activated during cell migration using Raichu-Rap1. HAECs cultured as a monolayer sheet were transfected with plasmids expressing Raichu-Rap1 and time lapse-imaged under the phase-contrast and FRET view after scratching. Cells were moving into the wound as revealed by phase-contrast observations (Fig. 7, *left panels*). Cell expressing Raichu-Rap1 as well as untransfected cells moved toward the wound. Rap1 was activated at the membrane ruffles in the leading edge (Fig. 7, *right panels*), where Crk was localized at focal complexes or growing focal adhesions (Fig. 6). These results suggested that Crk-Rap1 signaling upon focal adhesion assembly may contribute to the directional migration.

Rap1-RAPL Signaling Is Required for Directional Movement during Wound Healing—To test whether Rap1 is required for wound healing, we examined the effect of inactivation of Rap1 by overexpression of rap1GAPII on the directional cell migration. Rap family consists of Rap1A, Rap1B, Rap2A, and Rap2B (1). These molecules share common GEFs and GAPs for their activation and inactivation, respectively. To examine the effect of the Rap family on wound healing, inactivation of Rap by rap1GAPII, a common GAP for all of the Rap family members (33), is preferable rather than knocking down these Rap molecules using the small interfering RNA technique. In addition, rap1GAPII is suitable for the inactivation of Rap1, because it is reported that Rap1N17 does not work as a dominant negative form of Rap1 (34). HUVECs cultured as a monolayer were infected with adenovirus expressing either EGFP or rap1GAPII for 24 h. Infection efficiency exceeded 90%, as confirmed by fluorescence microscopy (Fig. 8*C*). There was no difference in cell confluence between HUVECs expressing rap1GAPII and those expressing EGFP. The EGFP-expressing cells separated by the wound moved toward the center line of the wound, whereas rap1GAPII-expressing HUVECs did not. The wound was almost closed by mobilized EGFP-expressing HUVECs 24 h after scratching, whereas it was not closed by rap1GAPII-expressing HUVECs (Fig. 8*A*).

To test the requirement of Rap1-RAPL signaling for directional movement, we used the RA mutant of RAPL to interfere with the association of RAPL with Rap1. HUVECs expressing EGFP-RA mutant were compared with those expressing EGFP-RAPL during wound healing. HUVECs infected with EGFP-RAPL-expressing adenovirus closed the wound 24 h af-

balt3/zbc-bc/zbc-bc/zbc00605/zbc8644-05g eichelbt S=4 28/12/04 19:27 | 4/Color Figure(s) 2-8 | ARTNO: M409701200

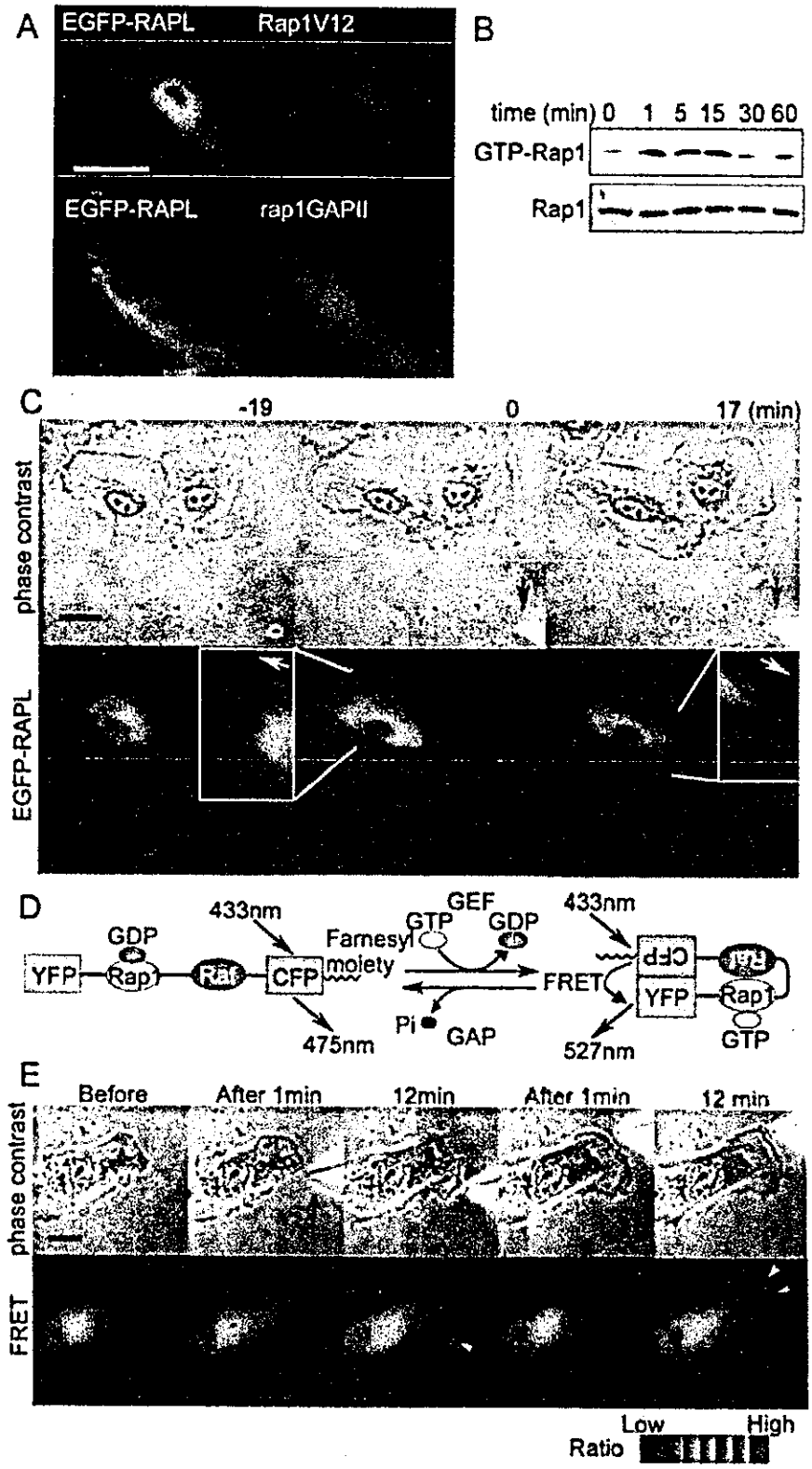

FIG. 5. **Rap1 regulates the localization of RAPL and precedes the extension of microtubules toward the leading edge of migrating cells upon chemotactic S1P stimulation.** *A*, HAECs were co-transfected with pCA-EGFP-RAPL and either pIRM21-Rap1V12 (*top*) or pIRM21-rap1GAPII (*bottom*). Note that EGFP-RAPL is dissociated from microtubules in Rap1V12-expressing cells, whereas EGFP-RAPL is associated with microtubules in rap1GAPII-expressing cells. *B*, HAECs stimulated with 1 μM S1P during the time period indicated at the *top* were lysed and analyzed by Bos's pull-down method using the GST-Rap1 binding domain of RalGDS. *C*, HAECs expressing EGFP-RAPL were time lapse-imaged before (−19 min) and after (17 min) the point (0) when 1 μM S1P was applied from a micropipette. Note that at time point 0, the cell

balt3/zbc-bc/zbc00605/zbc8644-05g eichelbt S=4 28/12/04 19:27 4/Color Figure(s) 2-8 ARTNO: M409701200

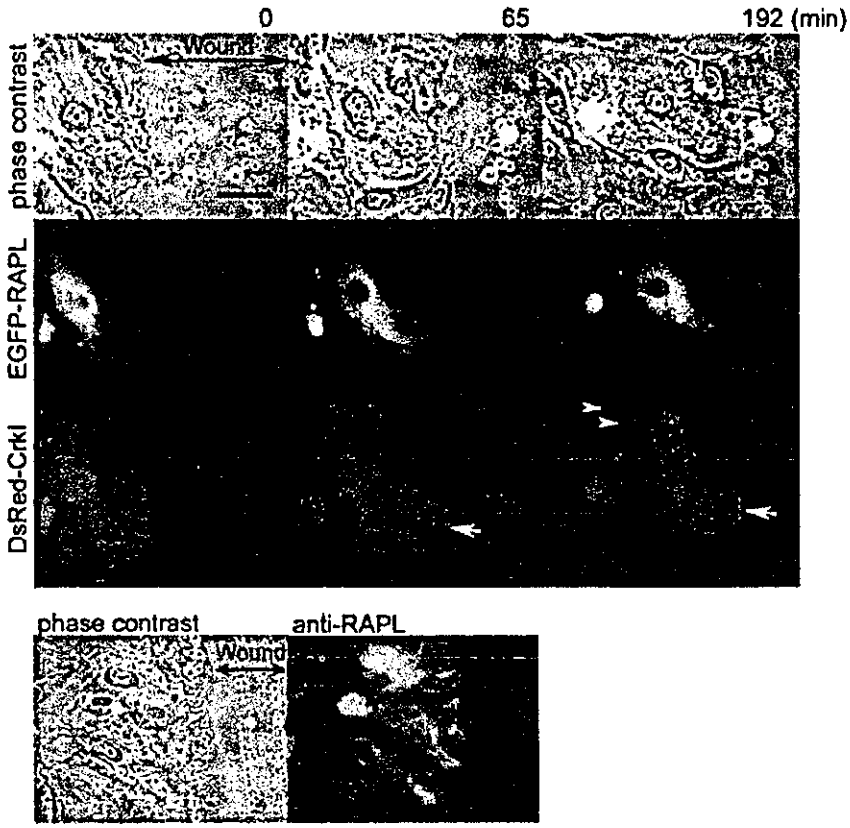

FIG. 6. **Microtubules marked by EGFP-RAPL grow toward the leading edge during wound healing.** *A*, monolayer-cultured HAECs expressing both EGFP-RAPL and DsRed-CrkI were time lapse-imaged after scratching. Phase-contrast (*top*), EGFP (*middle*), and DsRed (*bottom*) images were obtained through Olympus IX81 fluorescent microscope at the time point after scratching as indicated at the *top*. The *arrows* in the *bottom panel* indicate the nascent focal complexes at the leading edge, whereas the *arrowheads* indicate the focal adhesions in the retracting region. Note that microtubules marked by EGFP-RAPL grow toward the leading edge marked by DsRed-CrkI. *Wound*, scratched area. *Bar*, 50 μm. A series of time lapse images of phase-contrast, EGFP, and DsRed view were converted to a video (Supplemental Video 7). *B*, monolayer-cultured HAECs were immunostained with anti-RAPL 4 h after scratching. Phase contrast (*left*) and immunostaining with anti-RAPL (*right*) followed by visualization with Alexa488-conjugated secondary antibody are shown.

ter scratching, whereas those infected with EGFP-RA mutant-expressing adenovirus did not (Fig. 8*B*). To exclude the possibility that RA mutant-expressing cells moved more slowly than EGFP-expressing cells, we monitored randomly migrating cells expressing either RA mutant or EGFP. There was no significant change of the migratory velocity between two groups (Supplemental Fig. 2*C*). These data indicated that Rap1 activation and subsequent Rap1-RAPL association is required for directional movement of endothelial cells during wound healing.

DISCUSSION

The directional migration is accompanied with microtubule growth toward the leading edge of migrating cells. The microtubule extension depends on the localization of microtubule-capturing or -attracting molecules. Microtubules cooperatively promote cell migration accompanied with cell polarization together with actin cytoskeleton (35, 36). Extracellular stimuli activating Rho family proteins, Rho, Rac, and Cdc42, via plasma membrane receptors and cell-ECM complexes determine the direction of microtubule growth (28). Therefore, the downstream effectors of Rho family proteins are proposed to function as microtubule-capturing molecules at the cell cortex. Such candidate systems include Cdc42-Par6-protein kinase Cζ-dynein and Rac/Cdc42-IQGAP-CLIP170 (35, 38). Here we demonstrate, for the first time, that Rap1-RAPL signaling contributes to determining the direction of cell migration accompanied with microtubule growth upon chemoattractant stimulation and during wound healing.

Given that RAPL was expressed in vascular endothelial cells and associated with GTP-Rap1, it is important to ask where and how RAPL is regulated by active Rap1 in living cells. To answer this question, we first examined the localization of RAPL and found that RAPL localized on microtubules from MTOC to the periphery. Previously, it has been reported that Rassf1A localizes on microtubules in a variety of cells (22) and participates in mitosis by inhibiting the binding of anaphase-promoting complex to Cdc20 (39) or by stabilizing microtubules for tumor suppression (22). Rassf members were originally isolated as a tumor suppressor. Thus, Rassfs have been mainly AQ: K

moving toward the left top corner exhibited microtubules growing in the same direction as the cell movement. An *enlarged image* is shown in the *white box* (*bottom left*). Upon start of the S1P application, the cell turn to the micropipette tip (*black arrows*), began to move and exhibited a protrusion toward the tip, in which the microtubules extended forward along the direction of movement. An *enlarged image* is shown in the *white box* (*bottom right*). The *white arrows* indicate the moving direction. A series of phase-contrast images and EGFP images were converted into a video (Supplemental Video 3). *Bar*, 40 μm. *D*, schematic illustration of Raichu-Rap1. FRET efficiency depends on the guanine nucleotide binding. GDP-bound Raichu-Rap1 emits 475-nm fluorescence when excited at 433 nm, whereas GTP-bound Raichu-Rap1 emits 527-nm fluorescence due to FRET. *Raf*, Ras/Rap1 binding domain of Raf. *E*, HAECs expressing Raichu-Rap1 were imaged during exposure to S1P from the micropipette tip. Phase-contrast images and FRET images were obtained before and after the S1P stimulation. The time points indicated at the *top* show the first location and stimulation with S1P (*black*), the relocation of the tip, and the stimulation with S1P (*red*). Note that increased FRET reflecting Rap1 activation was observed at the edge of protrusion toward the micropipette tip. *Red* and *blue hue* indicate the increased and decreased FRET, respectively. The *arrowheads* indicate the activated Rap1 shown by the increased FRET. A series of phase-contrast images and FRET images were converted to a video (Supplemental Video 4). HAECs expressing Raichu-Rap1N17 was FRET-imaged during exposure to S1P from the micropipette tip similarly to Raichu-Rap1. Note that FRET does not occur at the ruffled membrane induced by S1P (Supplemental Video 5). Untransfected HAECs do not exhibit membrane ruffles in response to S1P-free medium (Supplemental Video 6).

balt3/zbc-bc/zbc-bc/zbc00605/zbc8644-05g eichelbt S=4 28/12/04 19:27 4/Color Figure(s) 2-8 ARTNO: M409701200

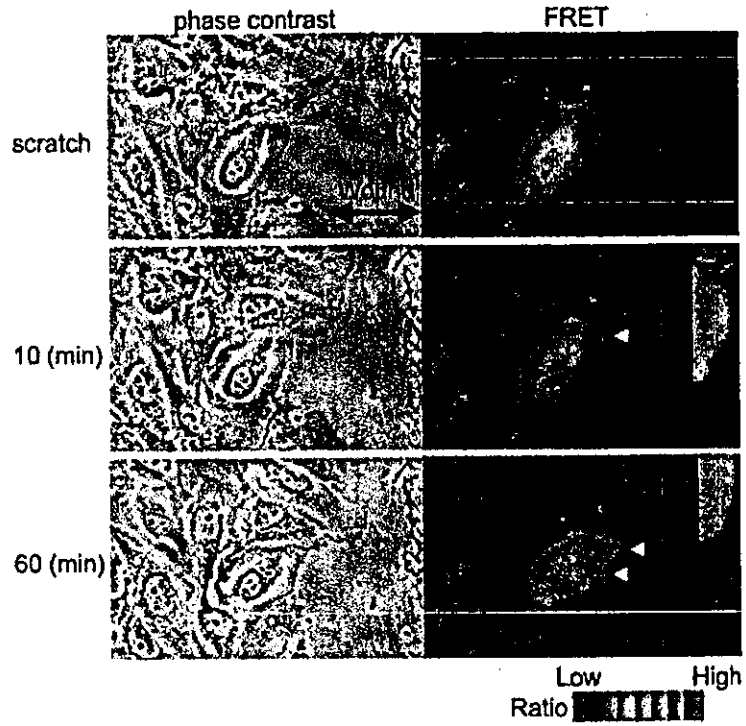

FIG. 7. **Rap1 is activated at the leading edge of the migrating cells.** HAECs cultured as a monolayer sheet transfected with pRaichu-Rap1 were scratched (*scratch*) and time lapse-imaged for phase-contrast and FRET observations. The elapsed time after scratching is indicated on the *left*. The *red hue* and *blue hue* in the FRET images indicate an increase (*high*) and a decrease (*low*) in the ratio of YFP to CFP, reflecting Rap1 activation and inactivation, respectively. The *arrowheads* indicate the activation of Rap1 at the leading edge of the cells migrating into the wound. The regions pointed out by the *arrows* are *enlarged* and shown in the *right corner* in the same *panel*. *Wound*, scratched area.

focused on as regulators of tumor suppression. We noticed that microtubules found in HAECs transfected with pEGFP-Rassf1A and -1C were different from those found in HAECs transfected with pCA-EGFP-RAPL. Rassf1 appeared to deform and thicken microtubules, whereas RAPL seemed to localize on endogenous microtubules. Recently, Rassf1A and -1C are reported to suppress tumors by stabilizing microtubules and maintaining genomic stability (40). The circular fibers found in the EGFP-Rassf1-expressing cells appear to reflect the stabilized microtubules. Furthermore, although Rassf1A-transfected cells exhibited the membrane ruffling, microtubules marked by EGFP-Rassf1A did not grow or shrink at all (Fig. 2 and Supplemental Videos 1 and 2, *left*). In clear contrast, EGFP-tagged RAPL and endogenous RAPL localizes on microtubules (Figs. 2*D* and 3 and Supplemental Videos 1 and 3, *right*). RAPL dislocated from microtubules when cells were transfected with Rap1V12-expressing plasmids (Fig. 5*A*). In addition, inactivation of Rap1 and disconnection between Rap1 and RAPL perturbed the directional migration (Fig. 8). These results imply that Rap1-RAPL signal may participate in regulation of microtubule growth. Further study is required to decipher the mechanism by which Rap1-RAPL-mediated signal regulates microtubule growth and/or stabilization.

Microtubules marked by EGFP-RAPL grew toward the leading edge, where DsRed-Crkl assembled as focal adhesions during wound healing. C3G is an Src homology 3 domain-binding protein of Crk and is required for stabilizing focal adhesions (7, 41). Thus, Rap1, a substrate of C3G, was likely to be activated at the assembly of focal adhesions. We used a FRET-based probe for visualizing Rap1 activation during wound healing. As expected, Rap1 was activated at the ruffled membrane where focal complexes were about to be assembled (Fig. 7). Thus, Rap1 activation at the leading edge preceded the directional migration. Rac1 activated downstream of CrkI via DOCK180 may tether microtubules through Rac1-binding protein, IQ-GAP1, and microtubule tip protein, CLIP-170 (42).

Microtubules have been suggested to target to focal adhesion, subsequently being captured and stabilized at focal adhesions (14, 15). We have not revealed the complex of Rap1-RAPL-microtubule at focal adhesions; however, Rap1 stabilizes focal adhesions, thereby indirectly contributing to the extension of microtubules. We have previously shown that Rap1 tightens the adhesion of cell-ECM complex (7) and that Rap1 is involved in maturation of focal complex to focal adhesions (24). RAPL was dislocated from the microtubules when constitutive active Rap1 was expressed (Fig. 5*A*). Katagiri *et al.* (16) reported that RAPL stabilizes the integrin-mediated cell attachment in lymphocytes stimulated with SDF-1. Accordingly, Rap1 activated at the focal adhesion may associate with RAPL, thereby stabilizing integrin-mediated focal adhesion to which microtubules target.

S1P triggers membrane ruffling, a hallmark of cell migration (26). We demonstrated that Rap1 was activated at S1P-induced membrane ruffling (Fig. 5). Membrane ruffling is the reorganization of actin by activated Rac. Rac activation downstream of Rap1 was previously reported in the Rap1-dependent secretory pathway (43). Rap1 promotes membrane extension by activating Rac via Vav2 and Tiam1 (44). Very recently, RIAM has been found to bind GTP-bound Rap1 and enhance integrin-mediated cell adhesion by regulating actin cytoskeleton (45). Thus, Rap1 appears to extend membranes by not only stabilizing integrin-mediated cell adhesion but activating Rac. Notably, microtubules marked by EGFP-RAPL grew toward locally activated Rap1 by S1P in the ruffled membrane. Although it is uncertain whether Rac activation is required for Rap1-RAPL-mediated signaling, Rac activation by S1P in parallel with or downstream of Rap1 may contribute to microtubule extension where RAPL localizes.

FRET-based probes, which can be introduced into living cells, have enabled us to monitor the spatial and temporal activation of signaling molecules: the activation of Ras superfamily members upon EGF-stimulation (4), the involvement of Crk in S1P-triggered signaling (26), and Rac activation during cell migration (37). We have previously shown that the phosphorylation of Crk was prominent at the S1P-induced membrane ruffling in vascular endothelial cells (26). Therefore, Rap1 activation by S1P in the present data is consistent with our previous data in that

balt3/zbc-bc/zbc-bc/zbc00605/zbc8644-05g eichelbt S=4 28/12/04 19:27 4/Color Figure(s) 2-8 ARTNO: M409701200

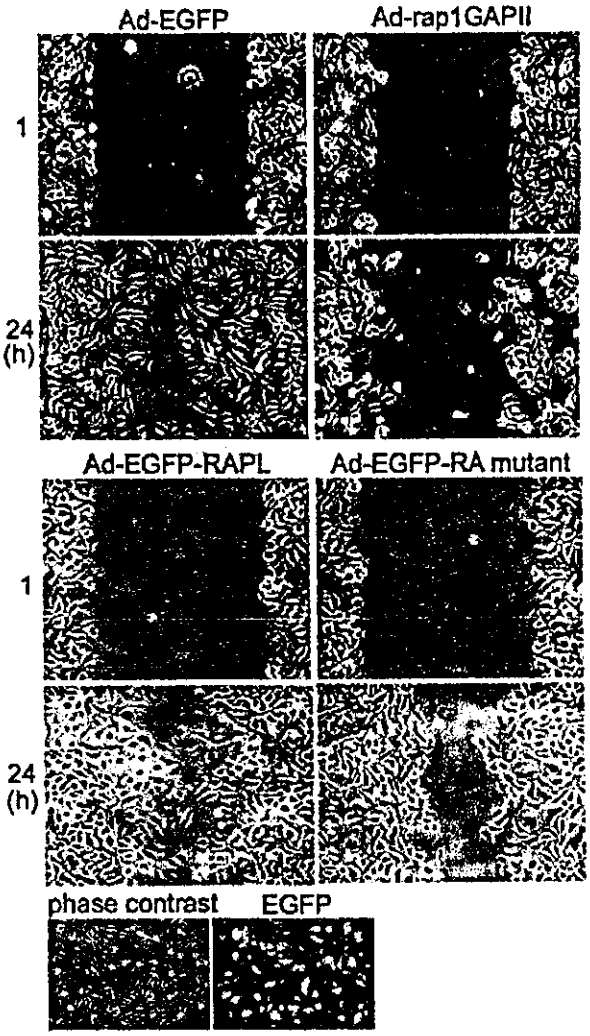

FIG. 8. **Rap1 activation and subsequent Rap1-RAPL association are required for wound healing.** *A*, HUVECs were either infected for 24 h with adenovirus expressing EGFP (Ad-EGFP) or adenovirus expressing rap1GAPII (Ad-rap1GAPII). 24 h after infection, the monolayer HUVECs were wounded by scratching. The wound healing was monitored at the time point as indicated on the *left*. Note that the cells expressing EGFP used as a control healed the wound, whereas the cells expressing rap1GAPII could not. HAECs infected with GFP-expressing adenovirus for 24 h were imaged. *B*, similarly to *A*, HUVECs were infected with either an adenovirus expressing EGFP-RAPL (Ad-EGFP-RAPL) or that expressing the EGFP-RA mutant of RAPL (Ad-EGFP-RA mutant). 24 h after scratching, cells were imaged. Note that the RAPL-expressing cells closed the wound, whereas those expressing RA mutant did not. *C*, the efficiency of infection was confirmed by the expression of EGFP in HUVECs infected with an adenovirus-expressing EGFP.

Crk-Rap1 signaling is triggered by S1P. During wound healing, Crk accumulated at focal adhesions and focal complexes near the leading edge. Although we could show Rap1 activation at the leading edge, it will be necessary to monitor the precise local activation of Rap1 at focal adhesions.

In conclusion, we have demonstrated that locally activated Rap1 regulates the directional cell migration accompanied by microtubule extension, presumably by dissociating RAPL from microtubules.

Acknowledgments—We thank M. Matsuda for advice; N. Yamagishi for the purified microtubules; H. Kurose and S. Hattori for the EGFP-expressing adenovirus and the rap1GAPII-expressing adenovirus, respectively; T. Kinashi for the anti-RAPL antibody; J. T. Pearson for critical reading of the manuscript; and M. Sone, M. Miyabayashi, K. Yamamoto, and N. Irisawa for technical assistance.

REFERENCES

1. Bos, J. L. (1998) *EMBO J.* **17**, 6776–6782
2. Bos, J. L., de Rooij, J., and Reedquist, K. A. (2001) *Nat. Rev. Mol. Cell. Biol.* **2**, 369–377
3. Ohba, Y., Kurokawa, K., and Matsuda, M. (2003) *EMBO J.* **22**, 859–869
4. Mochizuki, N., Yamashita, S., Kurokawa, K., Ohba, Y., Nagai, T., Miyawaki, A., and Matsuda, M. (2001) *Nature* **411**, 1065–1068
5. Reedquist, K. A., Ross, E., Koop, E. A., Wolthuis, R. M., Zwartkruis, F. J., van Kooyk, Y., Salmon, M., Buckley, C. D., and Bos, J. L. (2000) *J. Cell Biol.* **148**, 1151–1158
6. Katagiri, K., Hattori, M., Minato, N., Irie, S., Takatsu, K., and Kinashi, T. (2000) *Mol. Cell. Biol.* **20**, 1956–1969
7. Ohba, Y., Ikuta, K., Ogura, A., Matsuda, J., Mochizuki, N., Nagashima, K., Kurokawa, K., Mayer, B. J., Maki, K., Miyazaki, J., and Matsuda, M. (2001) *EMBO J.* **20**, 3333–3341
8. Kinbara, K., Goldfinger, L. E., Hansen, M., Chou, F. L., and Ginsberg, M. H. (2003) *Nat. Rev. Mol. Cell. Biol.* **4**, 767–776
9. Park, H. O., Sanson, A., and Herskowitz, I. (1999) *Genes Dev.* **13**, 1912–1917
10. Knox, A. L., and Brown, N. H. (2002) *Science* **295**, 1285–1288
11. Pollard, T. D., and Borisy, G. G. (2003) *Cell* **112**, 453–465
12. Ridley, A. J., Schwartz, M. A., Burridge, K., Firtel, R. A., Ginsberg, M. H., Borisy, G., Parsons, J. T., and Horwitz, A. R. (2003) *Science* **302**, 1704–1709
13. Small, J. V., Geiger, B., Kaverina, I., and Bershadsky, A. (2002) *Nat. Rev. Mol. Cell. Biol.* **3**, 957–964
14. Krylyshkina, O., Anderson, K. I., Kaverina, I., Upmann, I., Manstein, D. J., Small, J. V., and Toomre, D. K. (2003) *J. Cell Biol.* **161**, 853–859
15. Kaverina, I., Rottner, K., and Small, J. V. (1998) *J. Cell Biol.* **142**, 181–190
16. Katagiri, K., Maeda, A., Shimonaka, M., and Kinashi, T. (2003) *Nat. Immunol.* **4**, 741–748
17. Hesson, L., Dallol, A., Minna, J. D., Maher, E. R., and Latif, F. (2003) *Oncogene* **22**, 947–954
18. Vos, M. D., Martinez, A., Ellis, C. A., Vallecorsa, T., and Clark, G. J. (2003) *J. Biol. Chem.* **278**, 21938–21943
19. Vos, M. D., Ellis, C. A., Bell, A., Birrer, M. J., and Clark, G. J. (2000) *J. Biol. Chem.* **275**, 35669–35672
20. Vos, M. D., Ellis, C. A., Elam, C., Ulku, A. S., Taylor, B. J., and Clark, G. J. (2003) *J. Biol. Chem.* **278**, 28045–28051
21. Shivakumar, L., Minna, J., Sakamaki, T., Pestell, R., and White, M. A. (2002) *Mol. Cell. Biol.* **22**, 4309–4318
22. Liu, L., Tommasi, S., Lee, D. H., Dammann, R., and Pfeifer, G. P. (2003) *Oncogene* **22**, 8125–8136
23. Lee, M. J., Thangada, S., Paik, J. H., Sapkota, G. P., Ancellin, N., Chae, S. S., Wu, M., Morales-Ruiz, M., Sessa, W. C., Alessi, D. R., and Hla, T. (2001) *Mol. Cell* **8**, 693–704
24. Nagashima, K., Endo, A., Ogita, H., Kawana, A., Yamagishi, A., Kitabatake, A., Matsuda, M., and Mochizuki, N. (2002) *Mol. Biol. Cell* **13**, 4231–4242
25. Franke, B., Akkerman, J. W., and Bos, J. L. (1997) *EMBO J.* **16**, 252–259
26. Endo, A., Nagashima, K., Kurose, H., Mochizuki, S., Matsuda, M., and Mochizuki, N. (2002) *J. Biol. Chem.* **277**, 23747–23754
27. Kogata, N., Masuda, M., Kamioka, Y., Yamagishi, A., Endo, A., Okada, M., and Mochizuki, N. (2003) *Mol. Biol. Cell* **14**, 3553–3564
28. Wittmann, T., and Waterman-Storer, C. M. (2001) *J. Cell Sci.* **114**, 3795–3803
29. Schaller, M. D., and Parsons, J. T. (1995) *Mol. Cell. Biol.* **15**, 2635–2645
30. Vuori, K., Ilirai, H., Aizawa, S., and Ruoslahti, E. (1996) *Mol. Cell. Biol.* **16**, 2606–2613
31. Webb, D. J., Parsons, J. T., and Horwitz, A. F. (2002) *Nat. Cell Biol.* **4**, E97–E100 AQ: L
32. Kiyokawa, E., Mochizuki, N., Kurata, T., and Matsuda, M. (1997) *Crit. Rev. Oncog.* **8**, 329–342
33. Mochizuki, N., Ohba, Y., Kiyokawa, E., Kurata, T., Murakami, T., Ozaki, T., Kitabatake, A., Nagashima, K., and Matsuda, M. (1999) *Nature* **400**, 891–894
34. van den Berghe, N., Cool, R. H., Horn, G., and Wittinghofer, A. (1997) *Oncogene* **15**, 845–850
35. Rodriguez, O. C., Schaefer, A. W., Mandato, C. A., Forscher, P., Bement, W. M., and Waterman-Storer, C. M. (2003) *Nat. Cell Biol.* **5**, 599–609
36. Goode, B. L., Drubin, D. G., and Barnes, G. (2000) *Curr. Opin. Cell Biol.* **12**, 63–71
37. Itoh, R. E., Kurokawa, K., Ohba, Y., Yoshizaki, H., Mochizuki, N., and Matsuda, M. (2002) *Mol. Cell. Biol.* **22**, 6582–6591
38. Gundersen, G. G. (2002) *Nat. Rev. Mol. Cell. Biol.* **3**, 296–304
39. Song, M. S., Song, S. J., Ayad, N. G., Chang, J. S., Lee, J. H., Hong, H. K., Lee, H., Choi, N., Kim, J., Kim, H., Kim, J. W., Choi, E. J., Kirschner, M. W., and Lim, D. S. (2004) *Nat. Cell Biol.* **6**, 129–137
40. Vos, M. D., Martinez, A., Elam, C., Dallol, A., Taylor, B. J., Latif, F., and Clark, G. J. (2004) *Cancer Res.* **64**, 4244–4250
41. Caron, E., Self, A. J., and Hall, A. (2000) *Curr. Biol.* **10**, 974–978
42. Fukata, M., Watanabe, T., Noritake, J., Nakagawa, M., Yamaga, M., Kuroda, S., Matsuura, Y., Iwamatsu, A., Perez, F., and Kaibuchi, K. (2002) *Cell* **109**, 873–885
43. Mailliet, M., Robert, S. J., Cacquevel, M., Gastineau, M., Vivien, D., Bertoglio, J., Zugaza, J. L., Fischmeister, R., and Lezoualc'h, F. (2003) *Nat. Cell Biol.* **5**, 633–639
44. Arthur, W. T., Quilliam, L. A., and Cooper, J. A. (2004) *J. Cell Biol.* **167**, 111–122
45. Lafuente, E. M., van Puijenbroek, A. A., Krause, M., Carman, C. V., Freeman, G. J., Berezovskaya, A., Constantine, E., Springer, T. A., Gertler, F. B., and Boussiotis, V. A. (2004) *Dev. Cell* **7**, 585–595

MOLECULAR AND CELLULAR BIOLOGY, Jan. 2005, p. 136–146
0270-7306/05/$08.00+0 doi:10.1128/MCB.25.1.136–146.2005

Vol. 25, No. 1

Cyclic AMP Potentiates Vascular Endothelial Cadherin-Mediated Cell-Cell Contact To Enhance Endothelial Barrier Function through an Epac-Rap1 Signaling Pathway

Shigetomo Fukuhara,[1] Atsuko Sakurai,[1] Hideto Sano,[2] Akiko Yamagishi,[1] Satoshi Somekawa,[1,3] Nobuyuki Takakura,[2] Yoshihiko Saito,[3] Kenji Kangawa,[4] and Naoki Mochizuki[1]*

Department of Structural Analysis[1] and Department of Biochemistry,[4] National Cardiovascular Center Research Institute, Osaka, Department of Stem Cell Biology, Cancer Research Institute, Kanazawa University, Kanazawa,[2] and First Department of Internal Medicine, Nara Medical University, Nara,[3] Japan

Received 2 August 2004/Returned for modification 2 September 2004/Accepted 28 September 2004

Cyclic AMP (cAMP) is a well-known intracellular signaling molecule improving barrier function in vascular endothelial cells. Here, we delineate a novel cAMP-triggered signal that regulates the barrier function. We found that cAMP-elevating reagents, prostacyclin and forskolin, decreased cell permeability and enhanced vascular endothelial (VE) cadherin-dependent cell adhesion. Although the decreased permeability and the increased VE-cadherin-mediated adhesion by prostacyclin and forskolin were insensitive to a specific inhibitor for cAMP-dependent protein kinase, these effects were mimicked by 8-(4-chlorophenylthio)-2′-*O*-methyladenosine-3′, 5′-cyclic monophosphate, a specific activator for Epac, which is a novel cAMP-dependent guanine nucleotide exchange factor for Rap1. Thus, we investigated the effect of Rap1 on permeability and the VE-cadherin-mediated cell adhesion by expressing either constitutive active Rap1 or Rap1GAPII. Activation of Rap1 resulted in a decrease in permeability and enhancement of VE-cadherin-dependent cell adhesion, whereas inactivation of Rap1 had the counter effect. Furthermore, prostacyclin and forskolin induced cortical actin rearrangement in a Rap1-dependent manner. In conclusion, cAMP-Epac-Rap1 signaling promotes decreased cell permeability by enhancing VE-cadherin-mediated adhesion lined by the rearranged cortical actin.

Endothelial cells lining blood vessels regulate endothelial barrier function, which restricts the passage of plasma proteins and circulating cells across the endothelial cells. Endothelial barrier dysfunction results in an increase in vascular permeability, thereby causing edema or inflammatory or metastatic cell infiltration. Inflammatory mediators such as thrombin and histamine induce intercellular gap formation, leading to an increase in endothelial permeability (1, 4). In contrast, angiopoietin 1 and sphingosine-1-phosphate (S1P) stabilize endothelial barrier integrity (17, 18). In addition, cyclic AMP (cAMP), a second messenger downstream of Gs-coupled receptor, improves endothelial cell barrier function (32, 39, 43). Consistently, cAMP-elevating G protein-coupled receptor (GPCR) agonists, adrenomedullin (AM), prostacyclin (PGI2), prostaglandin E2 (PGE2), and β-adrenergic agonists reduce endothelial hyperpermeability induced by inflammatory stimuli (15, 19, 25).

The endothelial cell barrier is structurally organized by adherens junctions (AJ) and tight junctions. Vascular endothelial (VE) cells express both VE-cadherin (also known as cadherin-5 and CD144) and neural (N)-cadherin (9, 33). VE-cadherin constitutes AJ, whereas N-cadherin formed the cell-cell contacts between endothelial cells and endothelial cell-supporting pericytes. VE-cadherin mediates calcium-dependent, homophilic intercellular adhesion. Its short cytoplasmic tail binds to three armadillo family proteins, β-, γ-, and p120-catenins. β- and γ-catenins associated with α-catenin link the VE-cadherin complex to the actin cytoskeleton and, therefore, strengthen the AJ adhesiveness (9).

Endothelial AJ are dynamic structures, and their adhesive property is finely regulated by several different mechanisms. Tyrosine phosphorylation of VE-cadherin, β-catenin, and p120-catenin correlates with weakened endothelial cell-cell adhesion. VE growth factors and inflammatory mediators such as histamine and thrombin induce tyrosine phosphorylation of AJ components, resulting in the weakened cell-cell contacts and increased endothelial cell permeability (1, 14, 40). In clear contrast, angiopoietin 1, which stabilizes cell-cell contacts, induces dephosphorylation of endothelial cell adhesion molecules, VE-cadherin, and platelet endothelial cell adhesion molecule 1 (17). It has been also reported that S1P induces AJ formation and enhances barrier function through a Rac-dependent cortical actin rearrangement (18). cAMP-dependent protein kinase A (PKA) is suggested to be crucial for cAMP-triggered stabilization of cell-cell contacts and for barrier integrity of endothelial cells (43). However, it has not been clear whether PKA-independent signaling is involved in the regulation of endothelial barrier function.

Rap1, belonging to Ras family GTPase, is involved in the formation and stabilization of AJ in *Drosophila melanogaster* (23). Rap1 becomes the GTP-bound active form by guanine

* Corresponding author. Mailing address: Department of Structural Analysis, National Cardiovascular Center Research Institute, 5-7-1 Fujishirodai, Suita, Osaka 565-8565, Japan. Phone: 81-6-6833-5012, ext. 2508. Fax: 81-6-6835-5461. E-mail: nmochizu@ri.ncvc.go.jp.

nucleotide exchange factor (GEF) and the GDP-bound inactive form by GTPase-activating proteins (GAP), respectively. GEFs for Rap1 include C3G, CalDAG-GEFs, Epacs, and DOCK4 (reviewed in reference 6). DOCK4, which is disrupted in various types of human cancers, regulates the formation of AJ (41). Very recent reports also revealed that Rap1 activity is required for the formation of E-cadherin-based cell-cell contacts (20, 36). These findings prompted us to investigate how Rap1 is activated to stabilize cell-cell contacts and to examine the physiological consequence of stabilized cell-cell contacts by Rap1.

In the present study, we investigated the mechanism by which cAMP-elevating GPCR agonists potentiate endothelial barrier function and restrict cell permeability. We found that increased cAMP triggers Epac-Rap1 signaling to reduce permeability independently of PKA by augmentation of VE-cadherin-mediated cell-cell adhesion.

MATERIALS AND METHODS

Reagents and antibodies. Human recombinant AM was kindly provided by Shionogi & Co. Ltd (31). Materials were purchased as follows: isoproterenol (Iso), PGE2, PGI2, thrombin, forskolin (FSK), and 3-isobutyl-1-methylxanthine (IBMX) from Wako Pure Chemical Industries; dibutyryl-cAMP (dbcAMP) from Sigma-Aldrich; H89 from Seikagaku Corporation; 8-(4-chlorophenylthio)-2′-*O*-methyladenosine-3′,5′-cyclic monophosphate (8-CPT-2′-O-Me-cAMP) from Tocris; fluorescein isothiocyanate (FITC)-labeled dextran (molecular weight, 42,000) and purified human immunoglobulin G (IgG) Fc protein from ICN Biologicals; vascular endothelial growth factor (VEGF) from R & D Systems. Anti-Rap1GAPII antibody was developed by immunization of glutathione *S*-transferase (GST)-tagged Rap1GAPII (amino acids 411 to 694 of Rap1GAPII). Other antibodies used here were purchased as follows: anti-VE-cadherin from Chemicon International and Transduction Laboratories; anti-β-catenin from Transduction Laboratories; anti-CREB and anti-phospho-CREB (Ser133) from Cell Signaling Technology; anti-Rap1 from Santa Cruz Biotechnology; anti-cortactin from Upstate Biotechnology, Inc.; rhodamine-phalloidin and Alexa 488-labeled goat anti-mouse IgG from Molecular Probes; horseradish peroxidase-coupled goat anti-mouse and goat anti-rabbit IgG from Amersham Biosciences.

Cell culture and transfection. Human umbilical vein endothelial cells (HUVECs) and human arterial endothelial cells (HAECs) were purchased from Kurabo (Kurashiki, Japan). The cells were maintained in HuMedia-EG2 with a growth additive set as described previously (12) and used for experiments before passages 7 and 10, respectively. HEK293, 293T, and HeLa cells were maintained in Dulbecco's modified Eagle's medium (DMEM; Nissui, Tokyo, Japan) supplemented with 10% fetal bovine serum and antibiotics (100 μg of streptomycin/ml and 100 U of penicillin/ml). HUVECs and 293T cells were transfected by using Lipofectamine Plus reagent (Invitrogen) and by the calcium-phosphate precipitation technique, respectively.

Plasmids and adenovirus. pcDNA-VE-cad-Ect-Fc-His is a modified vector of pcDNA3.1-Fc-PECAM-1 (a kind gift from W. A. Muller, Cornell University) for producing the secreted form of the extracellular domain of VE-cadherin fused with Fc followed by a six-His tag. A DNA fragment encoding human Epac lacking the cAMP binding domain (amino acids 324 to 881) was amplified by PCR with pMT2SM-HA-Epac (a kind gift from J. L. Bos, Utrecht University, Utrecht, The Netherlands) as a template and ligated into the pCXN2 vector (12). pCXN2-FLAG-Rap1V12-IRES-EGFP expressed both FLAG-tagged Rap1V12 and internal ribosomal entry site (IRES)-driven enhanced green fluorescent protein (EGFP), and pCXN2-Rap1GAPII-IRES-EGFP expressed both FLAG-tagged Rap1GAPII and IRES-driven EGFP. pGL3 control vector was purchased from Promega Corp. Recombinant adenoviruses encoding Rap1GAPII (Ad-RapGAP) and LacZ (Ad-LacZ) were obtained from S. Hattori (The Institute of Medical Science, University of Tokyo) and M. Matsuda (Research Institute for Microbial Disease, Osaka University, Osaka, Japan), respectively. Adenoviruses expressing FLAG-tagged Rap1V12 and IRES-driven EGFP (Ad-Flag-Rap1V12-IRES-EGFP) were produced by using the Adeno-X system according to the manufacturer's protocol (Clontech). Endothelial cells were infected with adenoviruses at the appropriate multiplicities of infection (MOI) as described in the figure legends.

Permeability assay. Permeability across the endothelial cell monolayer was measured by using type I collagen-coated transwell units (6.5-mm diameter, 3.0-μm-pore-size polycarbonate filter; Corning Costar Corporation). HUVECs plated at 10^5 cells in each well were cultured for 3 to 4 days before experiments. After serum starvation in medium 199 containing 1% bovine serum albumin (BSA) for 1 h, the cells were treated with the agonists or drugs, as indicated in the figure legends, for 30 min. Permeability was measured by adding 1 mg of FITC-labeled dextran (molecular weight, 42,000)/ml together with or without 2 U of thrombin/ml to the upper chamber. After incubation for 30 min, 50 μl of sample from the lower compartment was diluted with 300 μl of phosphate-buffered saline (PBS) and measured for fluorescence at 520 nm when excited at 492 nm with a spectrophotometer F-4500 (Hitachi). HUVECs infected with adenovirus for 24 h after becoming confluent and kept for another 24 h in replaced medium were subjected to a cell permeability assay.

Immunocytochemistry. Monolayer-cultured HUVECs grown on a 35-mm-diameter glass base dish (Asahi Techno Glass) were starved in medium 199 containing 0.5% BSA for 3 h and subsequently incubated with the stimulants indicated in the figure legends for 30 min. After stimulation, the cells were fixed in PBS containing 2% formaldehyde for 30 min at 4°C, washed with PBS, and permeabilized with 0.05% Triton X-100 for 30 min at 4°C. Cells were blocked with PBS containing 4% BSA for 1 h at room temperature (RT) and stained with rhodamine-phalloidin for 20 min, anti-VE-cadherin for 60 min, and anticortactin for 60 min at RT. Protein reacting with antibody was visualized with Alexa 488-labeled goat anti-mouse IgG. Images were recorded with a confocal microscope (BX50WI, Fluoview; Olympus) with a water immersion objective lens (LUMPlanF1 100X1.00W).

VE-cadherin translocation assay and Western blot analysis. HUVECs plated in six-well plates were serum starved in medium 199 containing 1% BSA overnight. The cells were stimulated with PGI2 and FSK for the indicated time and fractionated with cytoskeleton-stabilizing buffer (10 mM HEPES [pH 7.4], 250 mM sucrose, 150 mM KCl, 1 mM EGTA, 3 mM $MgCl_2$, 1× protease inhibitor cocktail [Roche Diagnostics], 1 mM Na_3VO_4, 0.5% Triton X-100) by centrifugation at 15,000 × *g* for 15 min. The Triton X-100-insoluble fraction was subjected to sodium dodecyl sulfate-polyacrylamide gel electrophoresis (SDS-PAGE) followed by transfer to Immobilon-P (Amersham Biosciences) and immunoblotting with the indicated antibodies. Immunocomplexes were visualized by enhanced chemiluminescence detection (Amersham Biosciences) with species-matched peroxidase-conjugated secondary antibodies.

Purification of recombinant VE-cadherin ectodomain-Fc chimeric protein. 293T cells transfected with pcDNA-VE-cad-Ect-Fc-His were cultured in DMEM supplemented with 10% fetal calf serum for 24 h and subsequently kept in replaced medium (DMEM-F21 containing 1% fetal calf serum) for 7 days. VE-cadherin-Fc (VEC-Fc) protein secreted into the medium was collected every 2 days and centrifuged to remove floating cells and debris. VEC-Fc was collected on ProBond resin (Invitrogen) by gentle agitation overnight at 4°C. VEC-Fc protein bound to the beads was eluted with 500 mM imidazole, concentrated with Amicon Centriplus 30 (Millipore), and buffer exchanged into PBS containing 2 mM $CaCl_2$ and 2 mM $MgCl_2$ (PBS-Ca/Mg) by dialysis.

Cell adhesion assay. Twenty-four-well tissue culture plates were coated with 10 μg of VEC-Fc or Fc protein/ml in PBS-Ca/Mg at 4°C overnight. After washing with PBS-Ca/Mg, the plates were blocked with 1% heat-inactivated BSA in PBS (heat inactivated at 85°C for 12 min) for 1 h at RT. To examine cell adhesion to the VEC-Fc- or Fc-coated dish, cells were suspended in 0.5% BSA-containing medium 199 and incubated for 30 min at 37°C. Cells (1.5×10^5) were plated on each VEC-Fc- or Fc-coated well in the presence or absence of agonists, drugs, and 5 mM EGTA and adhered to the dish at 37°C for the indicated time. To analyze cell adhesion to a collagen-covered surface, cells were plated onto a collagen-coated six-well plate (Iwaki) and adhered to the dish in the presence or absence of 5 mM EGTA. After washing with PBS-Ca/Mg four times to remove nonadherent cells, adherent cells and input cells were quantified by measuring endogenous alkaline phosphatase activity as described elsewhere (35). Briefly, the cells were lysed in a buffer containing 100 mM Tris-citrate (pH 6.5) and 0.25% Triton X-100, and alkaline phosphate activity in the lysate was measured by using the AttoPhos AP fluorescent substrate system (Promega Corp.). To examine the effects of Rap1V12, EpacΔcAMP, and Rap1GAPII, HUVECs were transfected with plasmids encoding either Rap1V12, EpacΔcAMP, or Rap1GAPII together with the luciferase reporter construct (pGL3 control vector). The adhesion of cells expressing Rap1V12, EpacΔcAMP, or Rap1GAPII to the VEC-Fc-coated dish was normalized by measuring the luciferase activity of the cells and input cells (16).

Detection of GTP-bound form of Rap1. Rap1 activity was assessed by a modified Bos's method as described previously (34). Briefly, HUVECs starved in medium 199 containing 1% BSA overnight were stimulated with the indicated

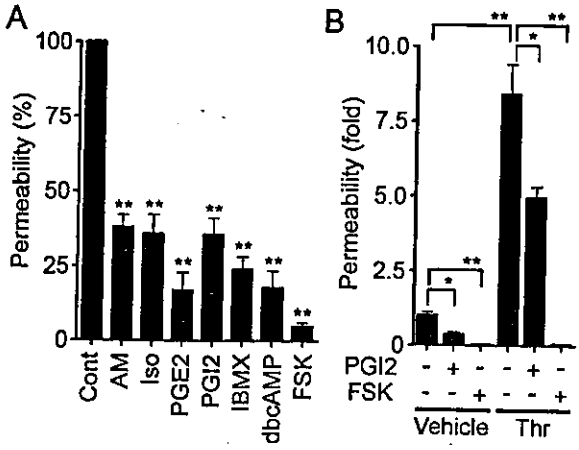

FIG. 1. cAMP enhances barrier function of monolayer VE cells. (A) Vascular permeability, reflecting barrier function, was analyzed by measuring the fluorescence of FITC-labeled dextran across the monolayer-cultured HUVECs as described in Materials and Methods. HUVECs grown on transwell filters were incubated with control (Cont), 0.1 μM AM, 200 μM Iso, 200-ng/ml PGE2, 10-μg/ml PGI2, 1 mM IBMX, 1 mM dbcAMP, and 10 μM FSK for 30 min. Average permeability ± standard deviation is expressed as a percentage compared to the control. (B) The effects of PGI2 and FSK on vascular permeability were quantified in the presence (+) or absence (−) (Vehicle) of 2 U of thrombin (Thr)/ml. Average permeability ± standard deviation is expressed as the increase relative to that observed in unstimulated HUVECs in the vehicle. Data shown are the results from at least three independent experiments. Significant differences from the control (A) or between two groups (B) determined by Student's *t* test are indicated by a single asterisk ($P < 0.05$) or double asterisks ($P < 0.01$).

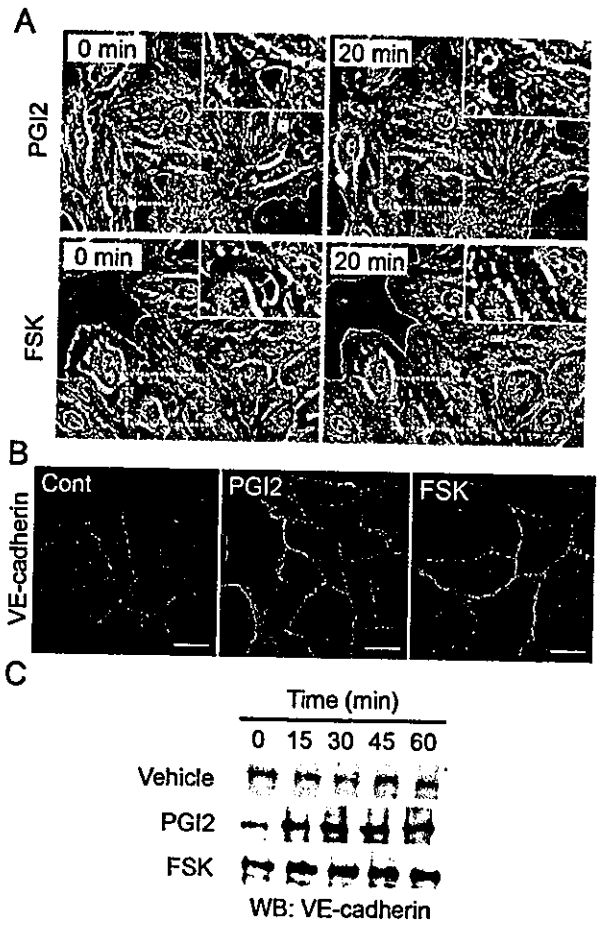

FIG. 2. cAMP induces AJ formation. (A) HUVECs cultured on a glass base dish were stimulated with 10 μg of PGI2/ml (upper panels) or with 10 μM FSK (lower panels) for 20 min and shown as phase-contrast images. Left and right panels show the cells before and after stimulation, respectively. The arrows indicate the sites of cell-cell contacts induced by PGI2 and FSK. The area boxed by the white broken line is enlarged in the right top of the panels. Bars, 50 μm. (B) Subconfluent HUVECs stimulated with vehicle (Cont), 10-μg/ml PGI2, and 10 μM FSK for 45 min were fixed, stained with anti-VE-cadherin antibody, and visualized with Alexa 488-conjugated secondary antibody through a confocal microscope (BX50WI; Olympus). Note that VE-cadherin (green) was accumulated at the cell-cell contact upon PGI2 and FSK stimulation. Bars, 50 μm. (C) Translocation of VE-cadherin was assessed by Triton X-100 solubility. HUVECs were stimulated with vehicle (top), 10-μg/ml PGI2 (middle), and 10 μM FSK (bottom) for the time indicated at the top and fractionated with cytoskeleton-stabilizing buffer as described in Materials and Methods. The Triton X-100-insoluble fraction was subjected to SDS-PAGE followed by Western blot analysis (WB) with anti-VE-cadherin.

agonists and drugs and lysed at 4°C in a pull-down lysis buffer (20 mM Tris-HCl [pH 7.5], 100 mM NaCl, 10 mM $MgCl_2$, 1% Triton X-100, 1 mM EGTA, 1 mM dithiothreitol, 1 mM Na_3VO_4, 1× protease inhibitor cocktail). GTP-bound Rap1 was collected on the GST-Rap1 binding domain of RalGDS precoupled to glutathione-Sepharose beads and subjected to SDS-PAGE followed by immunoblotting with anti-Rap1.

In vivo permeability assay. In vivo permeability was quantified by a modified Miles assay as described previously (29). In brief, ICR mice (Japan SLC, Inc.) shaved 3 days before experiments were lightly anesthetized and intravenously injected with 150 μl of 1% Evans blue dye solution (in saline) passed through a 0.22-μm-pore-size filter. Fifteen minutes later, 20 μl of PBS, VEGF (50 μg/ml), and/or 8-CPT-2′-O-Me-cAMP (1 mM) were applied by intradermal injections with a 30-gauge needle. The sites of intradermal injection were photographed 60 min after the injection, carefully dissected, and weighed. To quantify the vascular permeability, extravasated blue dye was eluted from the dissected skin with formamide at 56°C, and optical density was measured by spectrophotometry at 620 nm.

RESULTS

cAMP enhances the barrier property of monolayer-cultured endothelial cell. To evaluate the barrier function, we examined the permeability of FITC-labeled dextran across monolayer HUVECs. Expectedly, AM, Iso, PGE2, and PGI2 reduced basal endothelial permeability in HUVECs (Fig. 1A). PGI2 also reduced thrombin-induced vascular permeability (Fig. 1B). Other cAMP-elevating bio-ligands similarly reduced thrombin-induced permeability (data not shown). The bio-ligands for cAMP-elevating GPCR that we used in this study indeed increased cAMP in HUVECs (data not shown). Furthermore, IBMX (an inhibitor for phosphodiesterase), dbcAMP (a membrane-permeable cAMP analogue), and FSK (an adenylyl cyclase activator) resulted in a reduction of both basal and thrombin-induced endothelial permeability (Fig. 1; data not shown).

cAMP potentiates formation of AJ. Endothelial barrier function is largely dependent upon endothelial cell junctions. To investigate how cAMP affects AJ formation, we examined AJ organization by immunostaining with anti-VE-cadherin before and after stimulation. When subconfluent HUVECs with intercellular gaps were stimulated with PGI2 or FSK, the cells extended the plasma membrane and established cell-cell contacts with neighboring cells (Fig. 2A). Similar results were

obtained with AM and PGE2 (data not shown). Stimulation of HUVECs with PGI2 and FSK dramatically enhanced accumulation of VE-cadherin at cell-cell contacts (Fig. 2B).

The maturation of AJ requires homophilic binding of intercellular VE-cadherins and tight anchoring to the actin cytoskeleton via the cytoplasmic region through catenins. VE-cadherin anchored to the actin cytoskeleton is detected in detergent-insoluble fractions of cell lysates (26). We found an increase in VE-cadherin in the Triton X-100-insoluble fraction after stimulation with PGI2 or FSK (Fig. 2C). These results suggest that cAMP-elevating GPCR agonists potentiate AJ formation, which results in a cAMP-induced decrease in permeability.

cAMP promotes VE-cadherin-dependent endothelial cell adhesion. VE-cadherin is required for AJ formation (9). To test the involvement of a homophilic interaction of VE-cadherin in cAMP-enhanced AJ formation, we directly examined VE-cadherin-mediated cell adhesion. To mimic the VE-cadherin-dependent cell adhesion, we used VEC-Fc chimeric protein, which consisted of the extracellular domain of VE-cadherin fused to the Fc portion of immunoglobulin. HUVECs were plated onto VEC-Fc-coated dishes and time-lapse imaged. Cells attached within 5 min to the VEC-Fc-coated dish, subsequently spread, and exhibited a typical fried-egg morphology characterized by a large circular lamellipodium (Fig. 3A). No cells attached to the Fc-coated dish (Fig. 3B and C). Since cadherin-dependent cell adhesion requires Ca^{2+}, we examined the effect of Ca^{2+} chelation on cell adhesion to VEC-Fc-coated dishes. Cell adhesion to VEC-Fc-coated dishes was completely abolished by chelating extracellular Ca^{2+}, although cell attachment to the collagen-coated dish was unaffected (Fig. 3C and D). Basal and FSK-augmented cell adhesion to VEC-Fc-coated dishes was inhibited by EGTA (Fig. 3C). Both HUVECs and HAECs expressing VE-cadherin adhered to the VEC-Fc-coated dish (Fig. 3E). In clear contrast, HeLa and HEK293 cells, which express N-cadherin, but not VE-cadherin (20, 42), did not adhere to the VEC-Fc-coated dish, although these cells could attach to the collagen-coated dish (Fig. 3E; data not shown). Collectively, these results indicate that endothelial cell adhesion to the VEC-Fc-coated dish depends upon the homophilic ligation of VE-cadherin.

We proceeded to investigate the effect of cAMP-elevating GPCR agonists on VE-cadherin-mediated cell adhesion. The adhesion of HUVECs plated in the presence of PGI2 or FSK was evaluated by the alkaline phosphatase activity of remaining cells after washing. PGI2 enhanced adhesion of HUVECs to the VEC-Fc-coated dish in a concentration-dependent manner (Fig. 4A) and in a time-dependent manner (Fig. 4B). In a time course analysis, we noticed that enhanced adhesion was observed 7 min after the plating (Fig. 4B). Other cAMP-elevating GPCR agonists, including AM, Iso, and PGE2, potentiated VE-cadherin-dependent cell adhesion (Fig. 4C). In addition, similarly enhanced cell adhesion to the VEC-Fc-coated dish was also observed in the cells treated with cAMP-elevating drugs such as IBMX, dbcAMP, and FSK (Fig. 4F). Like PGI2, the effect of FSK on cell adhesion to the VEC-Fc-coated dish was concentration dependent and time dependent (Fig. 4D and E). This cAMP-induced cell adhesion to the VEC-Fc-coated dish depends on the enhanced homophilic ligation of VE-cadherin because FSK did not augment endothelial adhe-

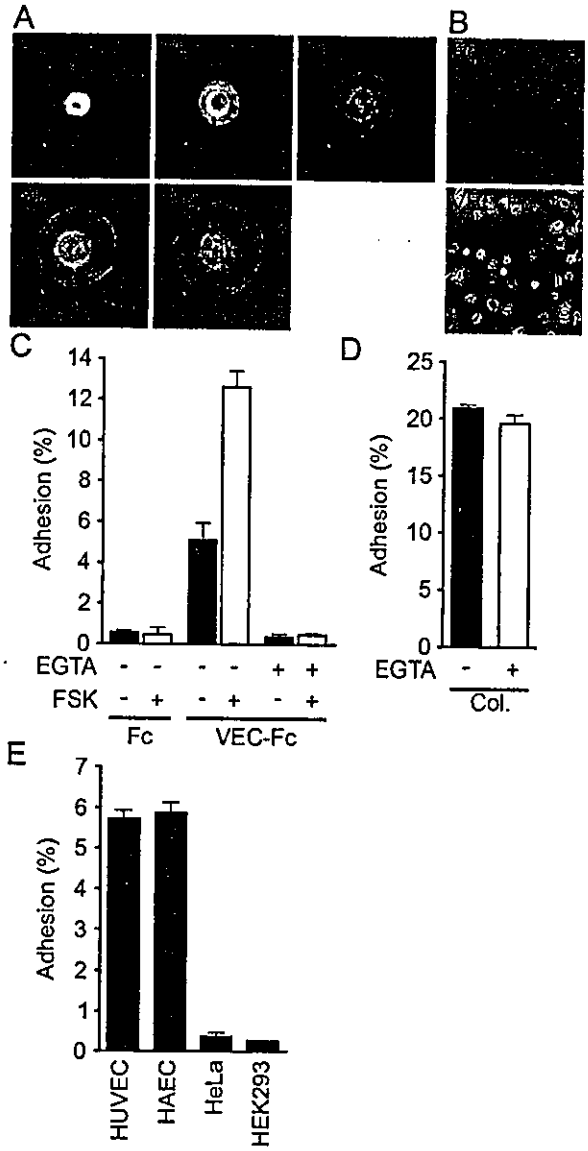

FIG. 3. Endothelial cells adhere to a VEC-Fc-coated dish through homophilic ligation of VE-cadherin. (A) HUVECs were plated onto the VEC-Fc-coated dish and time-lapse imaged at the time points (in minutes) indicated on the panels. Bar, 20 μM. (B) HUVECs were plated on the Fc-coated dish (top panel) or the VEC-Fc-coated dish (bottom panel) for 1 h and phase-contrast imaged after removal of nonadherent cells by washing with PBS-Ca/Mg. (C) HUVECs were plated onto either an Fc- or VEC-Fc-coated dish in the absence (−) or presence (+) of 5 mM EGTA and 10 μM FSK for 7 min. Cell adhesion was quantified as described in Materials and Methods. (D) Adhesion of HUVECs to a collagen-coated dish in the presence or absence of 5 mM EGTA was analyzed by a method similar to that described for panel C. (E) Adhesion of HUVECs, HAECs, and HeLa and HEK293 cells to the VEC-Fc-coated dish was examined as described in the legend for panel C. Cells adhering to the dishes of total input cells (percentage) is expressed as the mean ± standard deviation by measuring alkaline phosphatase activity of adherent cells divided by that of total input cells. Representative results from three independent experiments were shown in all panels.

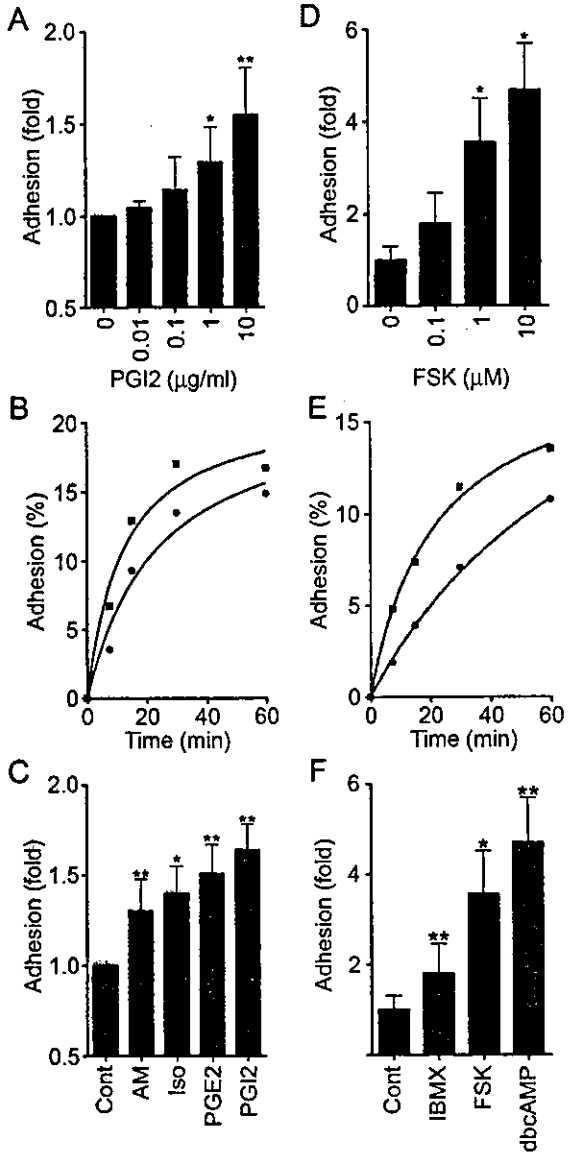

FIG. 4. cAMP potentiates VE-cadherin-dependent cell adhesion. (A) HUVECs were plated onto a VEC-Fc-coated dish in the presence of PGI2 at the concentrations indicated at the bottom for 7 min. Cell adhesion was quantified as described in Materials and Methods. Mean adhesion activity ± standard deviation is expressed as the increase compared with that observed in unstimulated cells. (B) HUVECs were plated onto the VEC-Fc-coated dish in the absence (circle) or presence (square) of 10-μg/ml PGI2 for the time indicated at the bottom. The percent adhesion was calculated by measuring the alkaline phosphatase activity of adherent cells divided by that of total input cells. (C) HUVECs stimulated with cAMP-elevating ligands similar to that described in the legend to panel A were assessed for adhesion activity. The concentration of stimulants was the same as described in the legend to Fig. 1A. (D) The effect of FSK on cell adhesion was analyzed by a method similar to that described for panel A, except that cells were preincubated for 10 min before plating. (E) The effect of 10 μM FSK on time-dependent adhesion was analyzed as described in the legend to panel B, except that cells were preincubated for 10 min before plating. (F) HUVECs stimulated with the reagent indicated at the same concentration used as described in the legend to Fig. 1A were analyzed for cell adhesion by a method similar to that described for panel D. Data are expressed as means ± standard deviations of the results from three independent experiments in panels A, C, D, and F. Representative results from three independent experiments were shown in panels B and E. A significant difference from the control determined by Student's *t* test is indicated with a single asterisk ($P < 0.05$) or double asterisks ($P < 0.01$).

sion to the Fc-coated dish or attachment to the VEC-Fc-coated dish in the absence of extracellular Ca^{2+} (Fig. 3C). These results indicate that cAMP potentiates VE-cadherin-dependent cell adhesion.

cAMP augments endothelial barrier function in a PKA-independent manner. PKA is suggested to be involved in cAMP-enhanced endothelial barrier function (43). Thus, we investigated the involvement of PKA in the regulation of endothelial barrier integrity by PGI2 and FSK. Unexpectedly, PGI2- and FSK-induced reduction of endothelial permeability was insensitive to a specific PKA inhibitor, H89 (7) (Fig. 5A and B). The reduction of thrombin-increased permeability by FSK was also unaffected by H89 (Fig. 5C). Consistently, H89 did not affect VE-cadherin-mediated cell adhesion enhancement by PGI2 and FSK (Fig. 5D and E). To confirm that H89 worked in HUVECs, we examined FSK-induced phosphorylation of CREB, a direct PKA substrate (38). Phosphorylation of CREB upon FSK stimulation was significantly inhibited by H89, indicating the effectiveness of this inhibitor in HUVECs (Fig. 5F). Therefore, these results apparently suggest a novel PKA-independent signaling pathway involved in cAMP-induced endothelial barrier function.

cAMP induces Rap1 activation. Besides PKA, Epac (cAMP-GEF) was identified as a novel cAMP target and a Rap1-specific GEF (5, 21). We therefore hypothesized that cAMP-activated Epac-Rap1 signaling is involved in the enhancement of VE-cadherin-dependent cell adhesion and endothelial barrier function. To address this possibility, we tested whether cAMP-elevating GPCR agonists induce Rap1 activation in HUVECs. Rap1 activity was determined by a pull-down assay by using a GST fusion protein of Rap1-binding domain of RalGDS according to the Bos's method. Bio-ligands for cAMP-elevating GPCR activated Rap1 (Fig. 6A). PGI2 rapidly induced Rap1 activation, which peaked at 1 to 5 min after the stimulation and then declined to the basal level by 10 min (Fig. 6C). A second wave of Rap1 activation was also observed 15 to 45 min after the stimulation (Fig. 6C). PGI2-induced Rap1 activation occurred in a concentration-dependent manner (Fig. 6B), which was associated with enhancement of VE-cadherin-dependent cell adhesion (Fig. 4A). Similarly, dbcAMP, FSK, and IBMX activated Rap1 (Fig. 6D). FSK-induced Rap1 activation reached a maximal level 2 to 5 min after the stimulation, and the level was sustained for up to 15 to 30 min (Fig. 6E). Collectively, these findings indicate that cAMP induces Rap1 activation in endothelial cells.

Specific activation of Epac reduces endothelial permeability and enhances VE-cadherin-dependent cell adhesion. To test whether the activation of endogenous Epac is sufficient to reduce endothelial permeability and to induce VE-cadherin-dependent cell adhesion, we used a recently developed cAMP analog, 8-CPT-2'-O-Me-cAMP, which specifically activates Epac without affecting PKA activity (13). As expected, 8-CPT-2'-O-Me-cAMP induced Rap1 activation in HUVECs (Fig. 7A), indicating that Epac is expressed in endothelial cells.

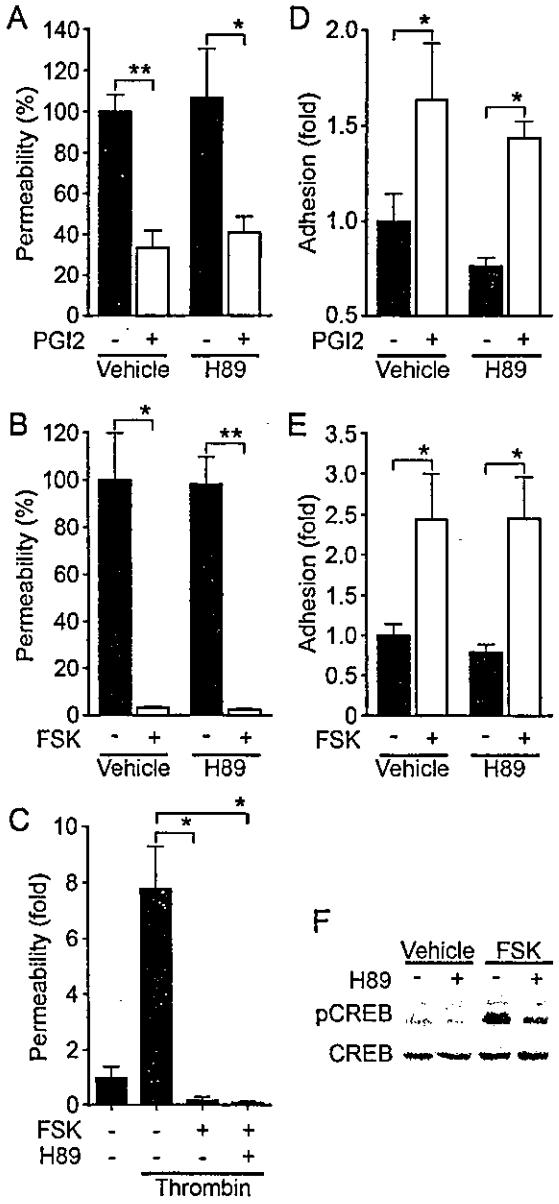

FIG. 5. cAMP-enhanced VE-cadherin-dependent cell adhesion and endothelial barrier function does not depend upon PKA. (A) Permeability across monolayer HUVECs grown on transwell filters were assessed by measuring FITC-labeled dextran as described in the legend to Fig. 1A. The effect of 10-μg/ml PGI2 on cell permeability without pretreatment (Vehicle) or with pretreatment with 5 μM H89, a specific PKA inhibitor, for 10 min is indicated as the percent permeability compared to that observed in untreated cells. +, present; −, absent. (B) The effect of 10 μM FSK on cell permeability without pretreatment (Vehicle) and with pretreatment with H89 was assessed similar to that described for panel A. (C) The effect of pretreatment of HUVECs with 5 μM H89 on FSK-induced reduction of 2-U/ml thrombin-induced permeability was analyzed. Permeability indicates the increase relative to that observed in untreated cells. (D) HUVECs untreated or pretreated with H89 for 10 min prior to stimulation with 10-μg/ml PGI2 were analyzed for cell adhesion as described in the legend to Fig. 4A. (E) HUVECs untreated or pretreated with H89 for 10 min prior to stimulation with 10 μM FSK were analyzed for cell adhesion as described in the legend to Fig. 4D. For panels A to E, data are expressed as means ± standard deviations of the results from triplicate samples. Similar results were obtained in at least three independent experiments. Significant differences between two groups determined by Student's t test are indicated by a single asterisk ($P < 0.05$) or double asterisks ($P < 0.01$). (F) HUVECs serum starved in 1% BSA-containing medium 199 for 6 h, followed by pretreatment with (+) or without (−) 5 μM H89 for 10 min, were stimulated with vehicle and 10 μM FSK for 10 min. Phosphorylation of CREB was assessed by Western blot analysis with anti-CREB (CREB) and anti-phospho-CREB-specific (pCREB) antibodies.

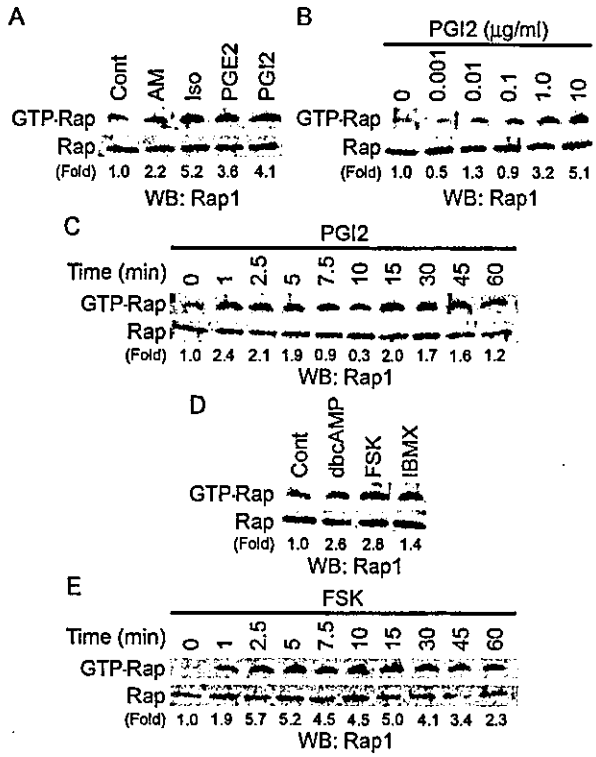

FIG. 6. cAMP induces Rap1 activation. (A) Serum-starved HUVECs kept in medium 199 containing 1% BSA overnight were stimulated with cAMP-elevating agonists for 2.5 min as indicated at the top and at the concentrations described in the legend to Fig. 1A. GTP-bound Rap1 was detected by pull-down assay as described in Materials and Methods. Activation indicates the ratio of the poststimulation GTP-Rap1 intensity of total Rap1 intensity to the prestimulation GTP-Rap1 intensity of total Rap1 intensity. (B) Rap1 activation was analyzed by detecting GTP-bound Rap1 with lysates from HUVECs stimulated with PGI2 for 2.5 min at the different concentrations indicated at the top. (C) Rap1 activation was analyzed by detecting GTP-bound Rap1 with lysates from cells stimulated with 10-μg/ml PGI2 for the time period indicated at the top. (D) Serum-starved HUVECs similar to those described in the legend to panel A were stimulated with the reagents indicated at the top for 10 min at the same concentrations described in the legend to Fig. 1A. Rap1 activation was assessed by a method similar to that described for panel A. (E) The effect of 10 μM FSK on time-dependent Rap1 activity was examined as described for panel C. Representative results from at least three independent experiments are shown for all panels.

8-CPT-2′-O-Me-cAMP dramatically reduced basal endothelial permeability, as did FSK and dbcAMP (Fig. 7B). Thrombin-induced permeability was also inhibited by 8-CPT-2′-O-Me-cAMP (Fig. 7C). Furthermore, we examined the effect of 8-CPT-2′-Me-cAMP on in vivo vascular permeability. VEGF-induced vascular permeability was completely blocked by coinjection of 8-CPT-2′-O-Me-cAMP (Fig. 7D). In addition, adhesion

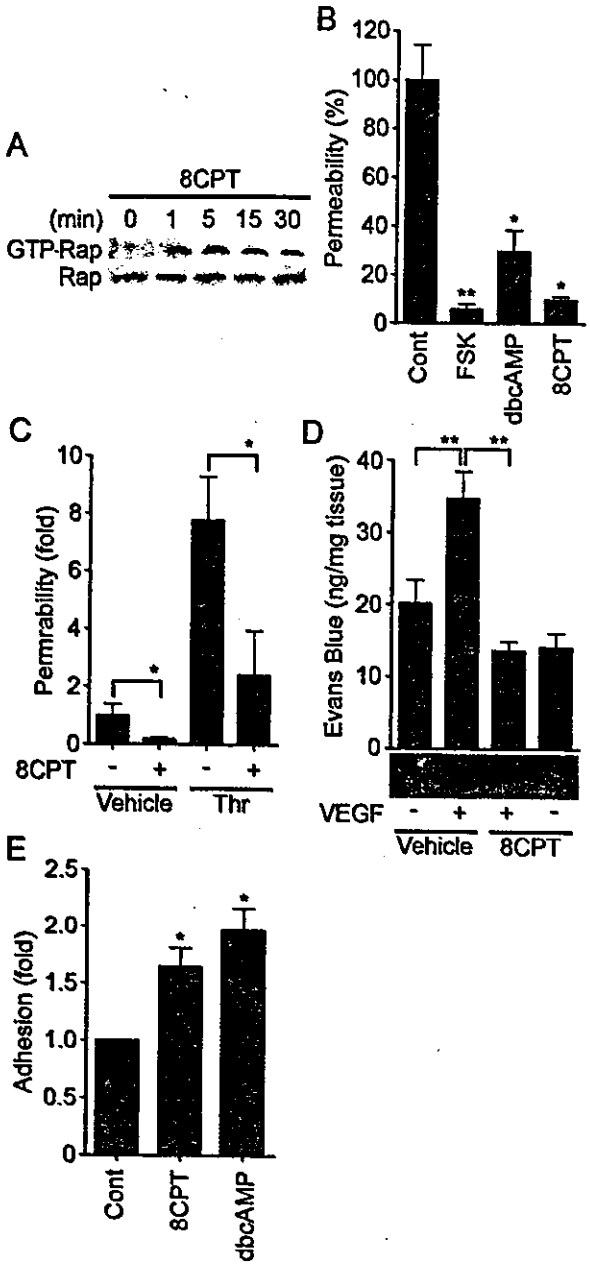

FIG. 7. Activation of Epac is sufficient to enhance VE-cadherin-dependent cell adhesion and endothelial barrier function. (A) Serum-starved HUVECs in medium 199 containing 1% BSA were stimulated with 0.2 mM 8-CPT-2′-O-Me-cAMP (8CPT) for the indicated time. Rap1 activity was determined as described in the legend to Fig. 6A. The result is a representative from three independent experiments. (B) Permeability of cells treated with the reagents as indicated on the bottom for 30 min was analyzed as described in the legend to Fig. 1A. (C) The effect of 0.2 mM 8CPT-2′-O-Me-cAMP on 2-U/ml thrombin-induced permeability was analyzed as described in the legend to Fig. 1B. (D) Effect of 8CPT-2′-O-Me-cAMP on VEGF-induced permeability was assessed by intradermal Miles assay as described in Materials and Methods. Amounts of extravasation of Evan blue in mouse dermal skin were measured 60 min after intradermal injection of vehicle and VEGF together with (+) or without (−) 8CPT. Mean leakage ± standard deviation of the results from 6 mice per group is expressed as nanograms of weight of extravasated Evans blue per milligram of weight of dermal skin. A photograph on the bottom shows leakage of Evans blue in dermal skin. (E) HUVEC adhesion to the VEC-Fc-coated dish in the presence of 0.2 mM 8CPT and 1 mM dbcAMP for 7 min was analyzed as described in the legend to Fig. 4F. In panels B, C, and E, data are expressed as means ± standard deviations of the results from triplicate samples. A significant difference from the control in panels B and E or between two groups in panels C and D was determined by Student's *t* test and indicated by a single asterisk ($P < 0.05$) or double asterisks ($P < 0.01$).

of HUVECs to the VEC-Fc-coated dish was significantly enhanced by 8-CPT-2′-O-Me-cAMP (Fig. 7E). Hence, Epac activation is sufficient to enhance VE-cadherin-dependent cell adhesion and to augment endothelial barrier function in vitro and in vivo.

Rap1 activation is essential for VE-cadherin-dependent cell adhesion and endothelial barrier function. We next proceeded to investigate the role of Rap1 in VE-cadherin-dependent cell adhesion and endothelial barrier function. To examine the effect of Rap1 on cell permeability and VE-cadherin-mediated cell adhesion, we inactivated endogenous Rap1 by adenovirus-expressing Rap1GAPII (Ad-RapGAP), which specifically catalyzes the hydrolysis of GTP to GDP on Rap1 (30). As shown in Fig. 8A, endogenous Rap1 activity was almost completely suppressed by the expression of increasing amounts of Rap1GAPII in HUVECs. This Rap1 inactivation paralleled the increase in basal permeability (Fig. 8B) and the inhibition of cell adhesion to the VEC-Fc-coated dish (Fig. 8D). In contrast, a constitutively active Rap1, Rap1V12, reduced both basal and thrombin-increased cell permeability (Fig. 8C). VE-cadherin-mediated cell adhesion was also enhanced by Rap1V12 and EpacΔcAMP, a constitutively active mutant of Epac (Fig. 8D). Taken together, these results indicate that Rap1 activation is required for VE-cadherin-mediated cell adhesion and endothelial barrier function.

cAMP enhances VE-cadherin-dependent cell adhesion and endothelial barrier function by activating Rap1. To test the requirement for Rap1 in endothelial barrier enhancement by cAMP-elevating GPCR agonists, we infected HUVECs with Ad-RapGAP and examined the effect of inactivation of Rap1 on PGI2- and FSK-induced reduction of cell permeability. Although basal endothelial permeability was reduced by PGI2 and FSK (Fig. 9A and B), overexpression of Rap1GAPII increased not only basal but also PGI2- and FSK-reduced endothelial permeability, indicating the requirement of Rap1 activity for PGI2- and FSK-induced barrier enhancement. We also investigated the involvement of Rap1 in PGI2- and FSK-induced VE-cadherin-dependent cell adhesion. PGI2 and FSK augmented VE-cadherin-dependent cell adhesion of HUVECs infected with control adenovirus (Ad-LacZ); however, their effects were dramatically suppressed by overexpression of Rap1GAPII (Fig. 9C and D). These data demonstrate that cAMP enhances VE-cadherin-dependent cell adhesion and endothelial barrier functions by activating Rap1.

cAMP induces endothelial cortical actin rearrangement in a Rap1-dependent manner. Endothelial barrier function is largely dependent upon the actin cytoskeleton supporting junctional adhesion molecules (10). Thus, we examined the effect of cAMP on cortical actin polymerization and assembly of polymerized actin in a monolayer of endothelial cells. Cortactin, an actin-binding protein, is known to be implicated in cortical actin rearrangement (8) and suggested to regulate S1P-induced endothelial barrier enhancement (11). PGI2,

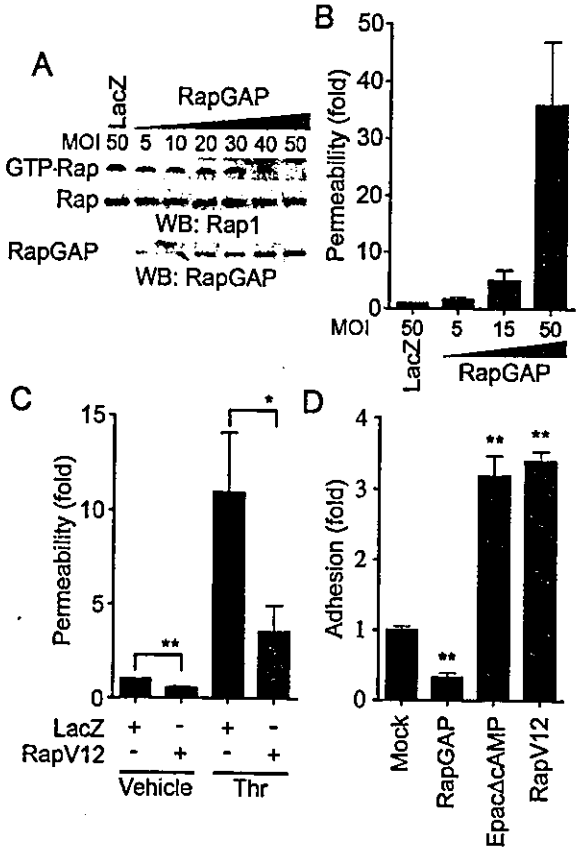

FIG. 8. Rap1 plays a critical role in VE-cadherin-dependent cell adhesion and endothelial barrier function. (A) Rap1 inactivation was assessed by detecting GTP-Rap1 in HUVECs infected with different MOI of adenovirus-expressing Rap1GAPII (RapGAP) as indicated at the top. An adenovirus-expressing LacZ at an MOI of 50 was used as a control. GTP-bound Rap1 (GTP-Rap) was detected by pull-down assay as described in Materials and Methods. Rap1 (Rap) and Rap1GAPII (RapGAP) expression were examined by Western blot analysis. (B) The permeability of FITC-dextran across HUVECs infected with adenovirus as indicated at the bottom was analyzed as described in Materials and Methods. Data are the means ± standard deviations of the results from three independent experiments and are expressed as increases relative to those of LacZ-infected cells. (C) Monolayer HUVECs infected with either an adenovirus-expressing LacZ or that expressing Rap1V12 at an MOI of 50 for 24 h were medium changed and cultured for another 24 h. The permeability of cells upon 2-U/ml thrombin stimulation (Thr) after starvation for 1 h was analyzed as described in the legend to Fig. 1B. Data are the means ± standard deviations of the results from five independent experiments and are expressed as inductions relative to those of untreated HUVECs infected with the LacZ-expressing virus. (D) HUVECs were transfected with either empty vector (Mock), plasmids expressing Rap1GAPII (RapGAP), EpacΔcAMP, or Rap1V12 together with the luciferase reporter construct. Transfected cells were plated on the VEC-Fc-coated dish and allowed to adhere for 15 min. Cell adhesion was analyzed as described in Materials and Methods. Data are expressed as increases compared to those of mock-transfected cells. The results indicate the means ± standard deviations of the results from triplicate samples. Similar results were obtained in three independent experiments. Significant differences between two groups in panel C or from the control in panel D are determined by Student's *t* test and are indicated by a single asterisk ($P < 0.05$) or double asterisks ($P < 0.01$).

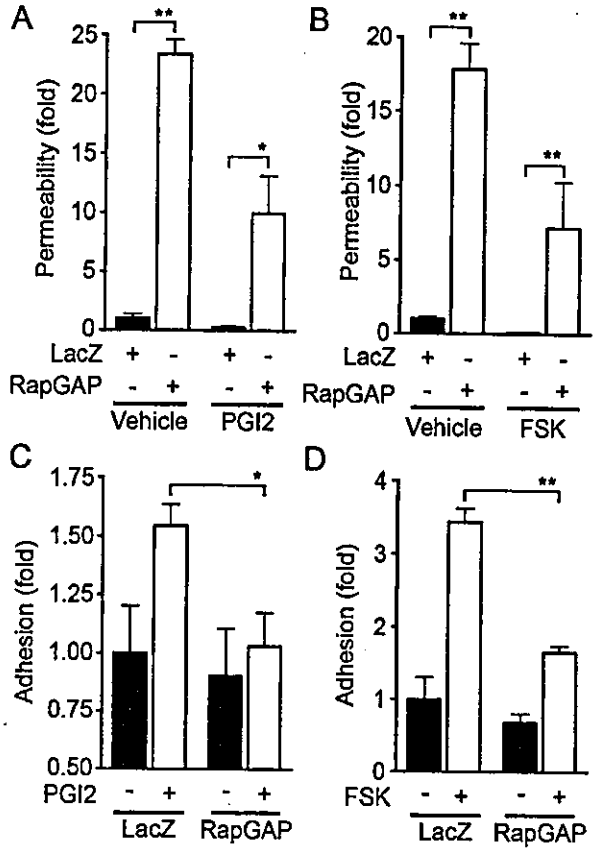

FIG. 9. Inactivation of Rap1 reduces PGI2- and FSK-induced barrier function and VE-cadherin-mediated cell adhesion. (A) Monolayer-cultured HUVECs grown on transwell filters were infected with either LacZ-expressing adenovirus (Ad-LacZ) or Rap1GAPII-expressing virus (Ad-RapGAP) at an MOI of 40 for 24 h. Medium was replaced with fresh medium after infection. Cells were cultured for an additional 24 h and treated with 10 μg of PGI2/ml for 30 min after serum starvation for 1 h. Permeability was analyzed as described in Materials and Methods. (B) The effect of 10 μM FSK on permeability in HUVECs infected with Ad-RapGAP was similarly analyzed. (C) HUVECs were infected with either Ad-LacZ or Ad-RapGAP at an MOI of 40 for 24 h. HUVECs resuspended in medium 199 with 0.5% BSA were plated onto VEC-Fc-coated dishes in the presence (+) or absence (−) of 10 μg of PGI2/ml for 7 min. Cell adhesion activity was quantified as described in the legend to Fig. 4A. (D) The effect of FSK on adhesion of HUVECs infected with Ad-RapGAP was analyzed similarly to that described for panel C. Resuspended HUVECs were preincubated with 10 μM FSK for 10 min before plating. Significant differences between two groups determined by Student's *t* test are indicated by a single asterisk ($P < 0.05$) or double asterisks ($P < 0.01$).

FSK, and 8-CPT-2'-O-Me-cAMP dramatically induced accumulation of polymerized actin and cortactin at cell-cell contacts (Fig. 10A). To explore the involvement of Rap1 in cAMP-mediated cortical actin rearrangement, an expression vector encoding Rap1GAPII was introduced into endothelial cells. FSK enhanced actin polymerization at cell-cell contacts in cells transfected with control vector encoding EGFP, whereas it did not in cells expressing Rap1GAPII (Fig. 10B). Cytochalasin D, an actin-depolymerizing agent, attenuated FSK-induced barrier enhancement (Fig. 10C) and inhibited FSK-induced VE-cadherin-dependent cell adhesion (Fig. 10D). These results suggest that the cortical actin rearrangement promoted by

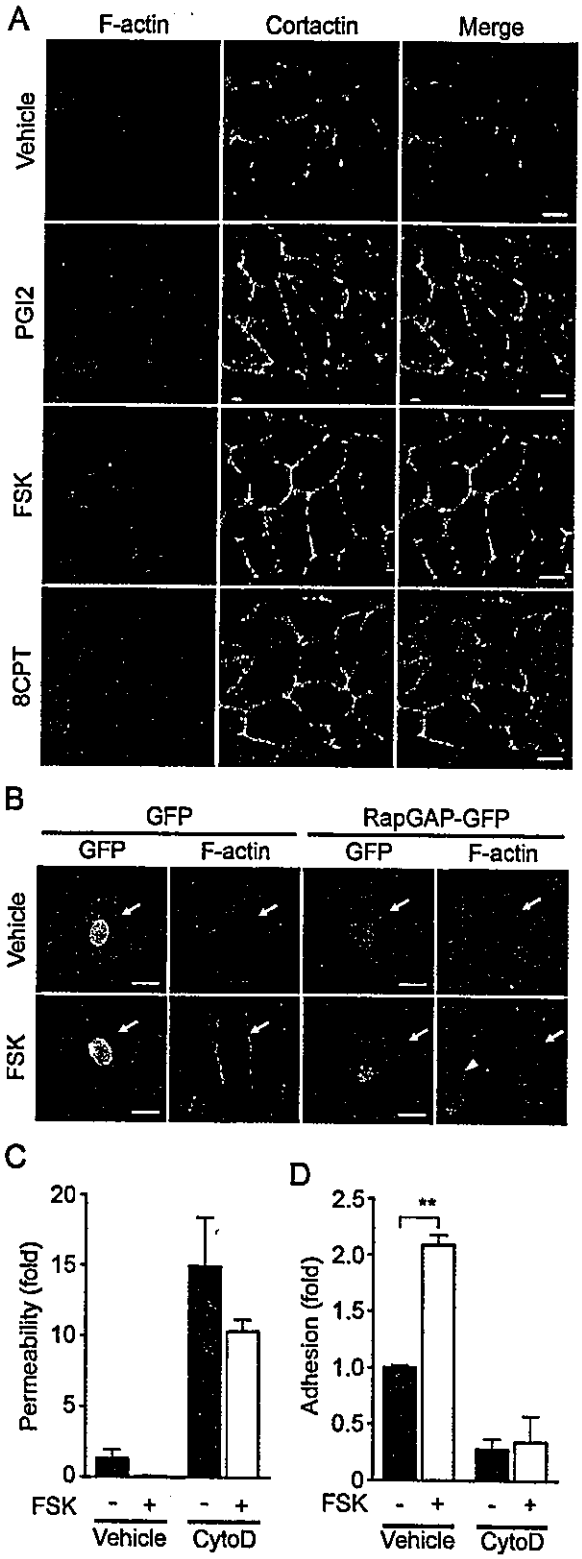

FIG. 10. cAMP induces cortical actin rearrangement in a Rap1-dependent manner. (A) Monolayer-cultured HUVECs starved in 0.5% BSA-containing medium 199 for 3 h were stimulated with vehicle (top row), 10-μg/ml PGI2 (second row), 10 μM FSK (third row), and 0.2 mM 8-CPT-2′-O-Me-cAMP (8CPT) (bottom row) for 30 min. Fixed and permeabilized cells were stained with rhodamine-phalloidin (left column) and with anti-cortactin (center column). Rhodamine images to detect F-actin (red) and Alexa 488 images for cortactin visualized by Alexa 488-labeled secondary antibody (green) were obtained through a confocal microscope (BX50WI). Right panels show the merged images of rhodamine and Alexa 488 images. Bars, 20 μm. (B) HUVECs transfected with an EGFP-expressing vector (left) and pCXN2-Rap1GAPII-IRES-EGFP (right) were serum starved in 0.5% BSA-containing medium 199 for 3 h and stimulated with vehicle (top panels) and 10 μM FSK (bottom panels). Cells were fixed, permeabilized, and stained with Rhodamine-phalloidin. EGFP images (green) and rhodamine images showing F-actin (red) were obtained similar to those in panel A. Arrows and arrowhead indicate transfected and untransfected cells, respectively. Bars, 20 μm. (C) Cell permeability of HUVECs pretreated with 2 μM cytochalasin D (CytoD) for 30 min followed by 10 μM FSK stimulation for 30 min was analyzed as described in the legend to Fig. 1A. −, absent; +, present. (D) The effect of pretreatment of 2 μM cytochalasin D (CytoD) on adhesion of HUVECs stimulated with FSK was analyzed as described in the legend to Fig. 5E. A significant difference between two groups determined by Student's t test is indicated by double asterisks ($P < 0.01$).

cAMP-Epac-Rap1 signaling may contribute to the potentiation of endothelial barrier function and VE-cadherin-dependent cell adhesion.

DISCUSSION

cAMP is a well-known intracellular signaling molecule that is capable of restoring diminished endothelial barrier function. Previous reports suggested that cAMP-induced barrier enhancement occurs through PKA (27, 39). In this study, however, we demonstrated a novel PKA-independent signaling pathway, the cAMP-Epac-Rap1 signaling pathway, involved in cAMP-induced barrier function based on the following observations. PGI2- and FSK-reduced endothelial permeability was insensitive to H89. A specific activator for Epac, 8-CPT-2′-O-Me-cAMP, reduced both basal and thrombin-increased permeability. Plasma leakage in response to VEGF was also inhibited by 8-CPT-2′-O-Me-cAMP in vivo. We found that the activation of Rap1 leads to decreased permeability. Not only all cAMP-elevating bio-ligands we tested but also FSK, db-cAMP, and IBMX activated Rap1. Consistently, cAMP-dependent Rap1 activation upon stimulation by these ligands involved Epac in the regulation of barrier function. A previous report showed that Rap1 is phosphorylated by PKA in neutrophils and platelets, although the function of phosphorylated Rap1 has not been elucidated (37). So far, Epac is known to regulate several biological functions including integrin-dependent cell adhesion, insulin secretion, and calcium release through ryanodine-sensitive Ca^{2+} channels (reviewed in reference 5). In addition to these Epac-mediated functions, we show, for the first time, that Epac-Rap1 signaling is important for regulation of endothelial barrier function.

AJ assembly contributes to the regulation of barrier function. Rap1 is involved in the formation and maintenance of AJ constituted by cadherin (23, 41). Recently, it has been reported that homophilic ligation of E-cadherin induced Rap1 activation, which may be responsible for maturation of AJ (20). Consistently, suppression of endogenous Rap1 inhibits formation of E-cadherin-dependent cell adhesion (36), suggesting the critical role of Rap1 in the establishment of cadherin-based cell-cell contacts. Here, we demonstrate that Rap1 also acts downstream of cAMP-Epac to potentiate VE-cadherin-depen-

dent cell adhesion, thereby improving barrier function. In addition to cAMP-elevating ligands, S1P, which enhances AJ formation and barrier function (18, 26), also activated Rap1 (our unpublished data). Thus, Rap1 may play a crucial role in barrier function induced by various types of barrier-improving factors.

Our data and previous studies show that cAMP protects thrombin-induced endothelial barrier dysfunction. cAMP does not limit the effect of thrombin on the initial loss of endothelial barrier (32). Instead, cAMP enhances the restoration of barrier function disrupted by thrombin. Recently, it was also reported that Cdc42 regulates the restoration of endothelial barrier function disrupted by thrombin (24). Thus, cAMP-Epac-Rap1 signaling may facilitate the formation of VE-cadherin-based cell-cell contacts, cooperatively or in parallel with Cdc42.

Rap1 enhances integrin-dependent cell adhesion in a variety of hematopoietic cells by modulating the affinity and avidity of integrin (6, 22). Cell adhesion to VEC-Fc-coated dishes was augmented by Rap1 activation, suggesting that the homophilic binding of VE-cadherin is also likely ascribed to the affinity and avidity of VE-cadherin modulated by Rap1-triggered inside out signaling. Hogan et al. reported that Rap1 activity is required for the targeting of E-cadherin molecules into nascent cell-cell contact sites, which in turn leads to the maturation of E-cadherin-based cell-cell contacts (20). Thus, cAMP-Epac-Rap1 signaling may also regulate the recruitment of VE-cadherin into maturing cell-cell contacts. Since downstream signaling of Rap1 that increases homophilic binding of VE-cadherin has not yet been characterized, the effector of cAMP-Epac-Rap1 signaling will need to be identified.

The actin cytoskeleton is a critical determinant of vascular integrity (10). PGI2, FSK, and 8-CPT-2′-O-Me-cAMP induced cortical actin rearrangement in a Rap1-dependent manner. FSK-induced VE-cadherin-dependent cell adhesion was inhibited by cytochalasin D. Thus, Rap1 may promote VE-cadherin-dependent cell adhesion by inducing cortical actin rearrangement. AF-6 may act downstream of Rap1 to regulate the actin cytoskeleton, since it binds to GTP-bound Rap1 and the actin cytoskeleton regulator, profilin, and is localized at AJ (2). Consistently, Canoe, the drosophila homolog of AF-6, and Rap1 function in the same molecular pathway during embryonic dorsal closure, which requires cell-cell contacts (3). S1P promotes endothelial barrier function by inducing Rac-dependent cortical actin rearrangement. S1P also induces Rap1 activation (our unpublished data). A previous report indicates that Rac can function downstream of Rap1 in the processing of the amyloid precursor protein (28). Taken together, Rac may act downstream of Rap1 to induce cortical actin rearrangement.

In conclusion, we have demonstrated that the cAMP-Epac-Rap1 signaling pathway promotes VE-cadherin-mediated cell adhesion and consequently improves endothelial barrier function.

ACKNOWLEDGMENTS

We thank J. L. Bos and W. A. Muller for plasmids, M. Matsuda and S. Hattori for adenovirus, J. T. Pearson for critical reading, and M. Sone, K. Yamamoto, and N. Irisawa for technical assistance.

This work was supported by grants from the Ministry of Health, Labor, and Welfare of Japan, from the Promotion of Fundamental Studies in Health Science of the Organization for Pharmaceutical Safety and Research of Japan, from the Ministry of Education, Science, Sports, and Culture of Japan, from the Uehara Memorial Foundation, and from Senri Life Science Foundation.

REFERENCES

1. **Andriopoulou, P., P. Navarro, A. Zanetti, M. G. Lampugnani, and E. Dejana.** 1999. Histamine induces tyrosine phosphorylation of endothelial cell-to-cell adherens junctions. Arterioscler. Thromb. Vasc. Biol. 19:2286–2297.
2. **Boettner, B., E. E. Govek, J. Cross, and L. Van Aelst.** 2000. The junctional multidomain protein AF-6 is a binding partner of the Rap1A GTPase and associates with the actin cytoskeletal regulator profilin. Proc. Natl. Acad. Sci. USA 97:9064–9069.
3. **Boettner, B., P. Harjes, S. Ishimaru, M. Heke, H. Q. Fan, Y. Qin, L. Van Aelst, and U. Gaul.** 2003. The AF-6 homolog canoe acts as a Rap1 effector during dorsal closure of the Drosophila embryo. Genetics 165:159–169.
4. **Bogatcheva, N. V., J. G. Garcia, and A. D. Verin.** 2002. Molecular mechanisms of thrombin-induced endothelial cell permeability. Biochemistry (Moscow) 67:75–84.
5. **Bos, J. L.** 2003. Epac: a new cAMP target and new avenues in cAMP research. Nat. Rev. Mol. Cell Biol. 4:733–738.
6. **Bos, J. L., J. de Rooij, and K. A. Reedquist.** 2001. Rap1 signalling: adhering to new models. Nat. Rev. Mol. Cell Biol. 2:369–377.
7. **Chijiwa, T., A. Mishima, M. Hagiwara, M. Sano, K. Hayashi, T. Inoue, K. Naito, T. Toshioka, and H. Hidaka.** 1990. Inhibition of forskolin-induced neurite outgrowth and protein phosphorylation by a newly synthesized selective inhibitor of cyclic AMP-dependent protein kinase, N-[2-(p-bromocinnamylamino)ethyl]-5-isoquinolinesulfonamide (H-89), of PC12D pheochromocytoma cells. J. Biol. Chem. 265:5267–5272.
8. **Daly, R. J.** 2004. Cortactin signalling and dynamic actin networks. Biochem. J. 382:13–25. [Online.] doi:10.1042/BJ20040737.
9. **Dejana, E.** 2004. Endothelial cell-cell junctions: happy together. Nat. Rev. Mol. Cell Biol. 5:261–270.
10. **Dudek, S. M., and J. G. Garcia.** 2001. Cytoskeletal regulation of pulmonary vascular permeability. J. Appl. Physiol. 91:1487–1500.
11. **Dudek, S. M., J. R. Jacobson, E. T. Chiang, K. G. Birukov, P. Wang, X. Zhan, and J. G. Garcia.** 2004. Pulmonary endothelial cell barrier enhancement by sphingosine 1-phosphate: roles for cortactin and myosin light chain kinase. J. Biol. Chem. 279:24692–24700.
12. **Endo, A., K. Nagashima, H. Kurose, S. Mochizuki, M. Matsuda, and N. Mochizuki.** 2002. Sphingosine 1-phosphate induces membrane ruffling and increases motility of human umbilical vein endothelial cells via vascular endothelial growth factor receptor and CrkII. J. Biol. Chem. 277:23747–23754.
13. **Enserink, J. M., A. E. Christensen, J. de Rooij, M. van Triest, F. Schwede, H. G. Genieser, S. O. Doskeland, J. L. Blank, and J. L. Bos.** 2002. A novel Epac-specific cAMP analogue demonstrates independent regulation of Rap1 and ERK. Nat. Cell Biol. 4:901–906.
14. **Esser, S., M. G. Lampugnani, M. Corada, E. Dejana, and W. Risau.** 1998. Vascular endothelial growth factor induces VE-cadherin tyrosine phosphorylation in endothelial cells. J. Cell Sci. 111(Pt 13):1853–1865.
15. **Farmer, P. J., S. G. Bernier, A. Lepage, G. Guillemette, D. Regoli, and P. Sirois.** 2001. Permeability of endothelial monolayers to albumin is increased by bradykinin and inhibited by prostaglandins. Am. J. Physiol. Lung Cell. Mol. Physiol. 280:L732–L738.
16. **Fukuhara, S., M. J. Marinissen, M. Chiariello, and J. S. Gutkind.** 2000. Signaling from G protein-coupled receptors to ERK5/Big MAPK 1 involves Galpha q and Galpha 12/13 families of heterotrimeric G proteins. Evidence for the existence of a novel Ras AND Rho-independent pathway. J. Biol. Chem. 275:21730–21736.
17. **Gamble, J. R., J. Drew, L. Trezise, A. Underwood, M. Parsons, L. Kasminkas, J. Rudge, G. Yancopoulos, and M. A. Vadas.** 2000. Angiopoietin-1 is an antipermeability and anti-inflammatory agent in vitro and targets cell junctions. Circ. Res. 87:603–607.
18. **Garcia, J. G., F. Liu, A. D. Verin, A. Birukova, M. A. Dechert, W. T. Gerthoffer, J. R. Bamberg, and D. English.** 2001. Sphingosine 1-phosphate promotes endothelial cell barrier integrity by Edg-dependent cytoskeletal rearrangement. J. Clin. Investig. 108:689–701.
19. **Hippenstiel, S., M. Witzenrath, B. Schmeck, A. Hocke, M. Krisp, M. Krull, J. Seybold, W. Seeger, W. Rascher, H. Schutte, and N. Suttorp.** 2002. Adrenomedullin reduces endothelial hyperpermeability. Circ. Res. 91:618–625.
20. **Hogan, C., N. Serpente, P. Cogram, C. R. Hosking, C. U. Bialucha, S. M. Feller, V. M. M. Braga, W. Birchmeier, and Y. Fujita.** 2004. Rap1 regulates the formation of E-cadherin-based cell-cell contacts. Mol. Cell. Biol. 24:6690–6700.
21. **Kawasaki, H., G. M. Springett, N. Mochizuki, S. Toki, M. Nakaya, M. Matsuda, D. E. Housman, and A. M. Graybiel.** 1998. A family of cAMP-binding proteins that directly activate Rap1. Science 282:2275–2279.
22. **Kinbara, K., L. E. Goldfinger, M. Hansen, F. L. Chou, and M. H. Ginsberg.**